
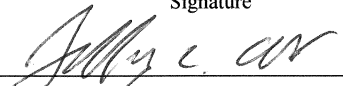
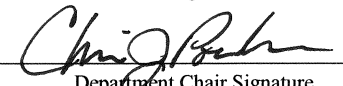


Daniel F Korfeh Jr.

The Chemistry of Magnetite from the Pea Ridge Iron Oxide Deposit, Missouri, U.S.A.

submitted in partial fulfillment of the requirements for the degree of
Master of Science in Earth and Environmental Sciences
Department of Earth and Environmental Sciences
The University of Michigan

 Signature	Accepted by: <u>Adam Simon</u> Name	<u>12/07/2016</u> Date
 Signature	<u>Jeffrey Alt</u> Name	<u>12/08/2016</u> Date
 Department Chair Signature	<u>Chris J. Poulsen</u> Name	<u>12/16/2016</u> Date

I hereby grant the University of Michigan, its heirs and assigns, the non-exclusive right to reproduce and distribute single copies of my thesis, in whole or in part, in any format. I represent and warrant to the University of Michigan that the thesis is an original work, does not infringe or violate any rights of others, and that I make these grants as the sole owner of the rights to my thesis. I understand that I will not receive royalties for any reproduction of this thesis.

- Permission granted.
- Permission granted to copy after: _____
- Permission declined.


Author Signature



The Chemistry of Magnetite from the Pea Ridge Iron Oxide Deposit, Missouri, U.S.A.

Daniel F Korfeh Jr.

Department of Earth and Environmental Sciences, University of Michigan,

1100 North University Avenue, Ann Arbor, MI 48109-1005 USA

December 5, 2016

Abstract

The Pea Ridge (PR) deposit is one of several iron oxide deposits hosted by a sequence of 1.45-1.48 Ga rhyolite tuffs of the St. Francois Mountain terrane in southeastern Missouri, USA. The deposit is characterized dominantly by magnetite and overprinted by secondary hematite. There is no consensus on how the deposit formed, with working hypotheses that include circulating basinal brines, meteoric fluids, magmatic-hydrothermal fluids, and immiscible iron oxide melt. In this study, we quantified the abundances of Ti, V, Ca, Al, and Mn for three generations of magnetite at Pea Ridge. Type 1 contains (± 1 sigma) 8.41 ± 1.24 wt. % Ti (range 5.7-12.4 wt. %), 790 ± 360 ppm V (range 120-1400 ppm), 290 ± 130 ppm Al (range 140-955 ppm), and 170 ± 70 ppm Mn (range 80-430 ppm). Type 2 magnetite contains (± 1 sigma) 0.456 ± 0.3 wt. % Ti (range 0.038-1.569 wt. %), 680 ± 220 ppm V (range 280-1030 ppm), 444 ± 500 ppm Al (range 130-2710 ppm) and 310 ± 190 ppm Mn (range 80-640 ppm). Type 3, the modally dominant generation of magnetite, contains (± 1 sigma) 390 ± 680 ppm Ti (range 60-6730 ppm), 486 ± 130 ppm V (range 90-1070 ppm), 520 ± 850 ppm Al (range 130-8980 ppm), and 440 ± 150 ppm Mn (range 80-910 ppm). When plotted on the [Ca+Al+Mn] vs. [Ti+V] discriminant diagram, Type 1 magnetite is comparable to igneous magnetite, whereas Type 2 and Type 3 scatter across the BIF, IOCG, and Kiruna fields. It is important to note that the stable Fe and O isotope ratios for the same magnetite samples from Pea Ridge (i.e., aggregates of magnetite grains that include Types 1, 2 and 3) are unequivocally magmatic in origin. In this thesis, it is suggested that Type 1 magnetite represents the original magnetite mineralization, which retains the magmatic Fe- and O-isotope signatures, and that post-mineralization dissolution and reprecipitation resulted in Types 2 and 3 magnetite with lower Ti concentrations and wide scatter

in V, Ca, Al, and Mn. Evidence for post-mineralized hydrothermal alteration is evinced by O-isotope data from zircon and quartz. The new data presented here support magmatic and magmatic-hydrothermal models for Pea Ridge.

Table of Content

Introduction	1
Geologic setting	2
<i>St. Francois Mountain Terrane</i>	2
<i>Pea Ridge Deposit</i>	3
Materials and methods	5
<i>Samples</i>	5
<i>Analytical Procedures</i>	5
Result	6
<i>Magnetite BSE and EDS Data</i>	6
<i>Magnetite Chemistry</i>	7
<i>Type 1 Magnetite</i>	7
<i>Type 2 Magnetite</i>	7
<i>Type 3 Magnetite</i>	8
Discussion	8
Conclusions	15
References	16
Figures	21
Tables	31

Introduction

The St. Francois Mountain terrane in southeastern Missouri, U.S.A. (Fig. 2), is predominantly characterized by 1.45-1.48 Ga (Bickford and Mose, 1975; Van Schmus et al., 1996) rhyolites, granites, and less abundant intermediate to mafic igneous rocks, which, together, host several iron oxide-apatite (IOA) ore deposits (Fig. 2) (Kisvarsanyi, 1981; Kisvarsanyi, 1990; Nuelle, 1991; Nold et al., 2013). The Pea Ridge deposit is one of several major IOA deposits hosted in the rhyolite ash flow tuffs of the St. Francois Mountain terrane (Kisvarsanyi and Proctor, 1967; Kisvarsanyi, 1981; Kisvarsanyi and Kisvarsanyi, 1989; Nold et al., 2014). Pea Ridge is modally dominated by magnetite (Fig. 3), with secondary hematite common throughout the deposit (Emery, 1968; Seeger et al., 2001). Pea Ridge was mined for magnetite from 1964 – 2001 (Nuelle et al., 1992; Seeger et al., 2001). Before the closure of the Pea Ridge deposit in 2001, approximately 41 Mt of iron were mined (Nuelle et al., 1992; Seeger et al., 2001; Nold et al., 2013). Current exploration activity at Pea Ridge is focused on the abundance of rare earth element (REE) enriched apatite; the deposit contains 600,000 tons of 12% REE proven reserves (Whitten and Yancey, 1990; Seeger et al., 2001). The Pea Ridge ore body has a nearly vertical shape and mineralization is structurally controlled. Field observations led mine geologists at Pea Ridge to refer to the deposit as a dike, although there is a lack of consensus for an igneous origin. There are four working genetic models for Pea Ridge, and IOA deposits in general: 1) a magmatic-hydrothermal fluid evolved from a silicate magma (e.g., Pollard, 2006; Nyström et al., 2008; Rieger et al., 2010, 2012; Jonsson et al., 2013; Knipping et al., 2015a, b; Childress et al., 2016); 2) non-magmatic hydrothermal fluids such as meteoric fluids or basinal brines driven by heat from either a magma body or the crustal geotherm (e.g., Barton and Johnson, 1996; Sillitoe and Burrows, 2002; Benavides et al., 2007); 3) metamorphic-hydrothermal fluids derived from metamorphic devolatilization (Fisher and Kendrick, 2008); and 4) a magmatic-hydrothermal

fluid evolved from a volatile-bearing iron oxide melt, which itself evolved via liquid immiscibility from a silicate magma (Barton, 2014). This thesis investigates the trace element chemistry of magnetite from Pea Ridge and uses the data to assess proposed genetic models for mineralization.

Geologic Setting

St. Francois Mountain Terrane

The St. Francois Mountain terrane consists of Mesoproterozoic igneous rocks that were emplaced or erupted over an area of 2500 km² in the Precambrian basement rocks of southeastern Missouri (Fig. 1, 2) (Kisvarsanyi and Kisvarsanyi, 1989). The St. Francois Mountain terrane consists of early Mesoproterozoic (ca. 1.50–1.44 Ga) volcanism and granite plutonism, and younger middle Mesoproterozoic (ca. 1.33–1.30 Ga) bimodal gabbro and granite plutonism (Day et al., 2016). Some studies propose that the St. Francois Mountain terrane formed in an anorogenic, intraplate setting in which felsic crustal material was subjected to partial melting (Hoffman, 1989; Kisvarsanyi and Kisvarsanyi, 1990), whereas other studies propose an orogenic, continental margin subduction zone environment at the southern margin of Laurentia (Menuge et al., 2002; River et al., 2000; Walker et al., 2002). Radiogenic isotope data (Nd-Sm and Lu-Hf) require a pre-existing felsic crust that was not more than 50 million years old at the time of formation of the St. Francois Mountain terrane (Ayuso et al., 2016). Incompatible trace element concentrations for the mafic igneous rock suite at the Silver Mines area are consistent with either a continental or island arc setting (Walker et al., 2002), and low Th/La ratios and Th contents are consistent with juvenile, mantle-derived mafic parental magmas that experienced little continental crust contamination (Day et al., 2016). Neodymium and Pb isotope data for igneous rocks that host and cross-cut IOA deposits in the district are consistent

with a depleted mantle source (Ayuso et al., 2016). Day et al. (2016) present new trace element data for igneous rocks and present a comprehensive review of published data from the St. Francois Mountain terrane. Those authors conclude that igneous activity in the St. Francois Mountain terrane involved anorogenic, within-plate magmatism, and continental subduction zone magmatism, and that ore mineralization was associated with the latter.

Pea Ridge Deposit

The Pea Ridge deposit is located in Washington County, Missouri, on the northern edge of the Ozark uplift (Fig. 2), a regional uplift zone covering ~40,000 mi² across Missouri, Arkansas, and Oklahoma. Surface outcrops and drill core samples indicate that the Pea Ridge deposit is hosted in high silica rhyolite ash flow tuffs (Seeger et al., 2001; Day et al., 2016). The Pea Ridge ore body strikes N60E and dips 75-90 SE (Nold et al., 2013), with a strike length of 2km and a thickness of 750m (Day et al., 2016). Mining activity extended to a depth of 410m (1345ft.) (Day et al., 2016), but the total depth of mineralization is not known (Seeger et al., 2001; Nold et al., 2013). The host ash flow tuffs strike N80W and dip 75 NW (Husman, 1989; Nuelle et al., 1992; Seeger et al., 2001; Day et al., 2016). The Pea Ridge deposit is divided paragenetically into four mappable zones (Fig. 3): 1) amphibole-quartz zones, 2) magnetite zones, 3) specular hematite zones, and 4) silicified zones (Emery, 1968; Husman, 1989; Sidder et al., 1993; Seeger et al., 2001). The magnetite zones are comprised of massive and brecciated magnetite (Seeger et al., 2001). The magnetite is fine grained, dense, and massive, with no foliation or lineation present. The massive magnetite has subconchoidal, finely crystalline and granular textures (Seeger et al., 2001; Nold et al., 2014). Hematite is common as grains pseudomorphic after magnetite, with the degree of replacement varying from minor rim alteration to complete replacement (Sidder et al., 1993). Specular hematite occurs as discrete

crystals, veinlets, irregular inclusions, and as crystals lining vugs (Nold et al., 2014). Abundant gangue minerals in the magnetite-rich ore zones include apatite, quartz, pyrite and monazite and modally less abundant phlogopite, amphibole, chlorite, fluorite, barite, chalcopyrite, and calcite (Seeger et al., 2001). In the brecciated parts of the Pea Ridge deposit, iron oxide ores have pseudobreccia to autobreccia textures (Day et al., 2016). The brecciated magnetite of the deposit is divided into magnetite-cemented heterolithic breccia and magnetite-cemented pseudo-breccia that contain matrices of predominantly hematite (Fig. 3) (Emery, 1968; Marikos et al., 1989). The magnetite-cemented heterolithic-breccia contains fragments of the host rhyolite volcanic rocks, chloritized rhyolite rocks and amphibole-quartz rocks, whereas the magnetite-cemented pseudo-breccia represents partial replacement of the host rhyolite rocks, wherein magnetite is present in breccia-like structures (Seeger et al., 2001). Along the margin of the main magnetite body (Fig. 3), the amphibole-quartz zones are developed. Massive coarse-grained actinolite and pods of quartz along with minor monazite, amphibole chlorite, chalcopyrite, pyrite, fluorite, barite and calcite are formed in the amphibole-quartz zones. The magnetite zones of the deposit are enveloped by discontinuous hematite zones found mostly along the footwall of the deposit. The hematite zones form gradational contacts with magnetite zones that are approximately 20-30m in width suggesting that they primarily formed as a result of alteration of magnetite zones (Seeger et al., 2001). The silicified zones are replacement features composed predominantly of quartz and minor K-feldspar and were emplaced after hematization of the deposit (Seeger et al., 2001; Nold et al., 2013). The silicified zones include minor amounts of fluorite, sericite, biotite, chlorite, pyrite, chalcopyrite, apatite, rutile, zircon, and hematite (Seeger et al., 2001).

There are four steeply dipping rare earth element (REE) – enriched breccia pipes that cut across the Pea Ridge magnetite ore body and volcanic host rocks (Emery, 1968; Nuelle et al.,

1991; Sidder et al., 1993) (Fig. 3). The REE-bearing breccia pipes are located in the footwall of the orebody and cross-cutting relationships indicate that the breccia pipes were emplaced after the silicified zones formed (Marikos et al., 1990; Seeger et al., 2001; Day et al., 2016). The primary REE bearing minerals in these pipes are monazite and xenotime, which are abundant as inclusions in apatite.

Materials and Methods

Samples

Twelve whole-rock ore samples were provided by J. W. Slack and W. C Day of the United States Geological Survey (USGS); details for each sample are provided in Table 1. The samples were collected from the high-grade, massive magnetite ore zone at varying depths from the surface of 2125, 2275, 2370, and 2440 ft. according to the maps of Seeger et al. (2001) (Fig. 3).

Analytical procedures

Ore samples were crushed to disaggregate magnetite grains, and a hand magnet was used to obtain sample fractions of pure magnetite. Samples were then placed on weighing paper on the stage of an optical microscope and individual grains of magnetite were handpicked with magnetic tweezers. Magnetite grains from each of the twelve hand samples were mounted in an epoxy resin, polished by using a sequence of diamond polishing pastes, and then carbon coated. The chemical compositions of magnetite grains were determined quantitatively by wavelength dispersive spectrometry (WDS) using the Cameca SX-100 electron probe microanalysis (EPMA) in the Electron Microbeam Analysis Laboratory (EMAL) housed in the Department of Earth & Environmental Sciences at the University of Michigan. The electron beam conditions of 20 keV of beam voltage, 30 uA of beam current and focused beam size were used to measure the

concentrations of the following elements: Fe, Mg, Al, Ca, Ti, V, Mn, Cr, and Si. The crystal standard and the counting time of each element are provided in Table 2. The calculated method detection limit (MDL) for the elements ranges from 20-120 ppm (Table 2); elemental concentrations below the MDL are not reported.

The JEOL JSM-7800F field emission scanning electron microscope (FE-SEM) in the EMAL facility was used to investigate chemical zonation in magnetite grains at resolutions as low as 1 μm . The FE-SEM was operated at a 15 keV beam voltage and a 20 nA beam current. The FE-SEM was used to acquire backscattered electron (BSE) images, and energy dispersive X-ray spectroscopy (EDS) elemental maps were acquired for the following elements: Fe, Ti, V, Ca, Si, Mn and Al.

Results

Magnetite BSE and EDS Data

The number of backscattered electrons (BSE) reaching a BSE detector is proportional to the mean atomic number of the sample. A brighter BSE intensity correlates with greater average atomic number of elements in the sample, whereas dark BSE intensity correlates with lower average atomic number. The BSE images acquired for Pea Ridge magnetite grains, in combination with EDS spot analyses, reveal three different types of magnetite, each indicated by a different relative brightness of the BSE image (Fig. 4). Magnetite in Figure 4 is labeled Type 1, Type 2 and Type 3, which increase in that order in brightness of the BSE intensity. Based on observations of BSE images of all analyzed magnetite grains, Type 3 magnetite is modally dominant, and Type 1 is the least abundant. The three types of magnetite are intimately intergrown with each other. In general, Type 1 magnetite is surrounded by Type 2 magnetite,

which is surrounded by Type 3 magnetite. The BSE images revealed the presence of exsolution features within Type 1 magnetite grains (Fig. 5).

The EDS element maps of Types 1, 2 and 3 magnetite grains indicate that the three types of magnetite grains have different trace element concentrations relative to one another. The EDS maps also reveal that the exsolution lamellae (Fig. 5) in Type 1 magnetite are enriched in Ti and V, both of which appear to be present in greater abundance than Fe. The EDS maps also show the concentrations of elements lower in the three types of magnetite (Fig 6). High concentrations of Ca indicate the presence of apatite inclusions in Type 3 magnetite grains (Fig. 6). The concentrations of Ca are below the detection limit in all three types of samples analyzed (Fig. 6).

Magnetite Chemistry

Major and trace element concentrations of magnetite samples are reported in Table 3. The data indicate that the three types of magnetite differ from one another in their trace element compositions, consistent with the observations made from the BSE and EDS maps. The compositions associated with each type of magnetite are described separately here.

Type 1 Magnetite

The trace element data are plotted in Figure 7. The average Fe concentration (± 1 sigma) in Type 1 magnetite is 59 ± 1.56 wt. % Fe. Type 1 magnetite contains (± 1 sigma) 8.41 ± 1.24 wt. % Ti, 790 ± 360 ppm V, 443 ± 272 ppm Mg, 290 ± 130 ppm Al, 170 ± 70 ppm Mn, and 131 ± 176 ppm Si. Calcium and Cr are below the EPMA detection limit in all the samples analyzed (Table 3). Attempts to quantify the composition of the exsolved lamellae were unsuccessful owing to overlap of the beam on the lamellae and host magnetite.

Type 2 Magnetite

The trace element data are plotted in Figure 7. The average Fe concentration (± 1 sigma) in Type 2 magnetite is 70 ± 1.5 wt. %. Type 2 magnetite contains (± 1 sigma) 0.456 ± 0.3 wt.% Ti, 677 ± 218 ppm V, 171 ± 200 ppm Mg, 453 ± 127 ppm Al, 294 ± 197 ppm Mn, and 780 ± 220 ppm Si. The concentrations of Al and Mn are similar to Type 1 magnetite (Fig. 7). Calcium and Cr are below the EPMA detection limit in all the samples analyzed (Table 3).

Type 3 Magnetite

The trace element data are plotted in Figure 7. The average Fe concentration (± 1 sigma) in Type 3 magnetite is 71 ± 1.29 wt. %. Type 3 magnetite contains (± 1 sigma) 390 ± 680 ppm Ti, 486 ± 130 ppm V, 240 ± 319 ppm Mg, 520 ± 850 ppm Al, 440 ± 150 ppm Mn, and 415 ± 175 ppm Si. Calcium and Cr are below the EPMA detection limit in all the samples analyzed (Table 3).

Discussion

Magnetite is a ubiquitous phase in many ore deposit types, as well as igneous, metamorphic and sedimentary rocks in general. Several recent studies have measured the trace element chemistry of magnetite from different ore deposit types and defined specific ranges of trace element concentrations of, e.g., Ti, V, Al, Mn, Ca for specific ore deposit types that allow magnetite to be used as a petrogenetic and provenance indicator (McClenaghan, 2005; Dupuis and Beaudoin, 2011; Dare et al., 2013; Nadoll et al., 2012; Dare et al., 2014; Nadoll et al., 2015). The trace elements Ti and V are grouped together, as are the concentrations of Al, Mn and Ca, to generate a plot in trace element space that discriminates magnetite from different ore deposit types. This, in turn, can be used to guide exploration strategies when sampling magnetite in greenfield environments, in provenance studies, as well as shed light on processes responsible for magnetite growth and post-mineralization alteration in a known ore deposit type (McClenaghan, 2005; Dupuis and Beaudoin, 2011; Nadoll et al., 2014; Dare et al., 2014).

The ability for trace element concentrations in magnetite to be used to discriminate magnetite from different environments is based fundamentally on the crystallographic structure of magnetite. Magnetite has the chemical formula Fe_3O_4 , or $\text{Fe}^{2+}\text{Fe}^{3+}_2\text{O}_4$, and has an inverse spinel structure, which is written as AB_2O_4 . (Fig. 8). The A site in magnetite is an octahedral site that generally accommodates divalent cations, whereas the B site is a tetrahedral site that generally accommodates trivalent cations. It has been shown that divalent cations such as Ni^{2+} , Mn, Co, Mg and Zn can substitute for Fe^{2+} in the A site, and trivalent cations such as Al, V, Mn and Ga can substitute for Fe^{3+} in the tetrahedral site (Fig. 8) (Lindsley, 1976; Wechsler et al., 1984; Dupuis, 2009; Dupuis and Beaudoin, 2011; Nadoll et al., 2014). Titanium (Ti^{4+}) can substitute into the tetrahedral B site by coupled substitution provided that a divalent cation substitutes into the A site to maintain charge balance (Wechsler et al., 1984; Goldschmidt, 1954). In general, the trace element composition of magnetite is dictated by the pressure and temperature conditions at the time of magnetite growth (Lindsley, 1991). The oxidation state of the system can also be important for substitution of polyvalent elements such as V, which is compatible in magnetite as V^{3+} in reduced systems, but not compatible as V^{5+} in oxidized systems. Other factors that control the trace element composition of magnetite include magma composition for igneous magnetite, and the chemistry of the hydrothermal fluid in the case of hydrothermal magnetite (Mollo et al., 2013; Nadoll et al., 2014; Hu et al., 2015).

The trace element chemistry data for magnetite from the Pea Ridge samples studied in this thesis are plotted on the $[\text{Ca}+\text{Al}+\text{Mn}]$ vs. $[\text{Ti}+\text{V}]$ compositional discriminant diagram in Figure 9. Each of the three types of magnetite is plotted as a different symbol. The various fields on this diagram are labelled based on the results of Dupuis and Beaudoin. (2011) and Nadoll et al. (2014). As mentioned above, Pea Ridge is classified as an iron oxide – apatite ore deposit,

and primary magnetite mineralization should plot in the Kiruna-IOA field on the discriminant diagram. While a small number of analyses of Type 2 magnetite do plot in the IOA field, the majority of the magnetite trace element data do not plot in the IOA field. The average composition for each type is indicated. The Type 1 average plots in the igneous field. The Type 2 average also plots in the igneous field, just outside the Kiruna field. The Type 3 average plots in the iron oxide – copper – gold (IOCG) field. The plot illustrates that there is a significant amount of variability within and among each of the three types of magnetite. For Type 1, there is less dispersion in [Ti+V] relative to [Ca+Al+Mn]. For Type 2, there is an equal order of magnitude variability in both [Ti+V] and [Ca+Al+Mn], and for Type 3, there is slightly more dispersion in [Ca+Al+Mn] relative to [Ti+V]. All of the analyses for Type 1 magnetite are consistent with the trace element chemistry for magnetite crystallized from silicate melts. The trace element chemistry of Type 2 magnetite varies from purely igneous, plotting in the (Fe-Ti, V) field, to purely Kiruna field, consistent with magnetite from unaltered IOA deposits, to low trace element concentrations that plot in the Undefined field. Type 3 magnetite grains plot in the fields for skarns, iron oxide – copper – gold (IOCG) deposits, banded iron formation (BIF) and in the undefined field.

Published studies of magnetite trace element chemistry indicate that, in general, there is a strong correlation between trace element chemistry and temperature. On the magnetite discriminant diagram (Fig. 9), magnetite that grows at high temperature plots in the upper right part of the diagram and magnetite grown at low temperature plots in the lower left part of the diagram. Nadoll et al. (2014) reported that magnetite with [Ti+V] > 0.1 wt. % and [Ca+Al+Mn] > 0.1 wt. % crystallized at temperatures of 300 to \geq 500 °C. These data correlate with the entire porphyry and Fe-Ti, V fields, and a small part of the skarn field. Magnetite with 0.005 to 0.1 wt.

% [Ti+V] and 0.01 to 0.8 wt. % [Ca+Al+Mn] crystallized at temperatures of 200 to 300 °C, and magnetite with <0.005 wt. % [Ti+V] and <0.09 wt. % [Ca+Al+Mn] crystallized at temperatures of <200 °C. These temperatures were determined by fluid inclusion microthermometry and other methods (Nadoll et al., 2014).

Knipping et al. (2015a, b) reported trace element chemistry (i.e., Ti, V, Mn, Ca, Al) for magnetite from the Los Colorados IOA deposit (Chile) that indicate that igneous magnetite that re-equilibrates, either during continual growth from an evolving magmatic/magmatic-hydrothermal fluid or via dissolution-reprecipitation, is enriched initially in [Ti+V] and [Ca+Al+Mn], and progressively becomes depleted in these trace elements. They documented that some individual grains of magnetite show a progressive change from high-temperature magnetite to low-temperature magnetite, where the trace element composition of the magnetite core plots in the igneous Fe-Ti, V field and outward toward the rim of the magnetite grain the trace element data plot in the porphyry, Kiruna, IOCG, and banded iron fields. The textural and compositional data for magnetite grains from the Pea Ridge magnetite deposit do not reveal such variation within individual grains. However, the three types of magnetite in the Pea Ridge ore body are consistent with preservation of high-temperature igneous, moderate to high-temperature magmatic-hydrothermal, and low-temperature hydrothermal processes.

The Ti concentrations and presence of ilmenite exsolution lamellae in Type 1 magnetite are consistent with Type 1 having crystallized from a silicate melt (Buddington and Lindsley, 1964). The trace element concentrations of Type 1 magnetite cluster in the Fe-Ti, V field on the discriminant plot (Fig. 9) and reveal that this generation of magnetite in the Pea Ridge deposit was associated with igneous activity. Ilmenite was not observed as a separate phase in any of the ore samples studied in this project. However, the presence of rutile in the ore samples has been

reported (Meighan et al., 2015). The presence of ilmenite exsolution lamellae is consistent with magnetite that grew from a silicate melt wherein all the Ti was initially dissolved in the magnetite structure. Subsequently, the Ti-magnetite experienced an increase in oxygen fugacity, which leads to Ti becoming incompatible in the structure of magnetite and exsolving as ilmenite (Buddington and Lindsley, 1964; Toplis and Carroll, 1995).

The trace element chemistry of Type 2 magnetite (moderate Ti) and Type 3 magnetite (modally dominant; depleted in Ti) are consistent with moderate to low-temperature growth of magnetite in the presence of a hydrothermal fluid (Nadoll et al., 2014). The discriminant diagram (Fig. 9) also shows the trace elements for both Types 2 and 3 spread across high temperature hydrothermal IOA-Kiruna field and the low temperature hydrothermal IOCG, BIF, and Skarn fields. Meighan et al. (2015) measured the Zr content of rutile grains and used the Zr-in-rutile thermometer to determine temperatures of formation for rutile that is paragenetically equivalent with magnetite from several parts of the Pea Ridge ore body. They report that rutile inclusions in Type 1 magnetite cores yield temperatures of $\leq 436 - 748$ °C, whereas temperatures in rutile grains in the magnetite rims and rutile in the matrix are $500 - 540$ °C. Zirconium-in-rutile temperatures for rutile grains in the silicified portion of the ore body range from $610 - 680$ °C. Meighan et al. (2015) also report Ti-in-quartz temperatures of $490 - 500$ °C for quartz inclusions in magnetite. These authors report Ti-in-quartz temperatures of $380 - 440$ °C for quartz in the matrix. These temperature data are consistent with interpretations of magnetite trace element chemistry plotted on the discriminant diagram; i.e., type 1 magnetite crystallized at the highest temperature, and types 2 and 3 magnetite crystallized second and third, respectively, at progressively lower temperature (Fig. 9) (Dupuis and Beaudoin, 2011; Nadoll et al., 2014).

The variation in trace element chemistry of the three types of magnetite in the Pea Ridge ore body (Fig. 9), and the range of temperatures determined by Ti-in-rutile and Ti-in-quartz thermometry, can plausibly be attributed to re-equilibration of primary, igneous magnetite with two separate pulses of hydrothermal fluid. Published $\delta^{18}\text{O}$ values for zircon from the St. Francois Mountain terrane range from 5.8‰ to 8.2‰ (average $\delta^{18}\text{O} = 7.3 \pm 1.1\text{‰}$), which are values typical for Proterozoic igneous rocks (i.e., $\delta^{18}\text{O} = 7.3 \pm 1.5\text{‰}$) (King et al., 2008). King et al. (2008) interpreted the $\delta^{18}\text{O}$ -zircon data to be the product of four separate hydrothermal alteration events that affected the Pea Ridge and surrounding systems. One hydrothermal event occurred prior to or synchronously with mineralization at Pea Ridge, and a second low-temperature hydrothermal event shortly after Pea Ridge mineralization. Those authors reported a $\delta^{18}\text{O}$ value of $+11.96 \pm 0.24\text{‰}$ for quartz from the brecciated (ore host) rhyolite in the Pilot Knob deposit that is higher than the regional average of $+8.7\text{‰}$ measured in individual quartz phenocrysts in igneous rocks. A $\delta^{18}\text{O}$ value of $+12\text{‰}$ is theoretically predicted for quartz in equilibrium with an intermediate to rhyolitic silicate melt of $+11\text{‰}$. Johnson et al. (2013; 2016) reported $\delta^{18}\text{O}$ values of $+13\text{‰}$ to $+20\text{‰}$ for quartz from the Pea Ridge deposit, which indicate an ore fluid that had a $\delta^{18}\text{O}$ value of $>10\text{‰}$. This $\delta^{18}\text{O}$ composition of the ore fluid was suggested by Johnson et al. (2013) to require the presence of an isotopically-heavy and externally-derived fluid in addition to a magmatic fluid. Childress et al. (2016) report new $\delta^{56}\text{Fe}$ data that unequivocally identify a magma source reservoir for Fe in Pea Ridge magnetite. Their data are shown in Figure 10. All of the Pea Ridge magnetite grains in their study have $\delta^{56}\text{Fe}$ values that overlap purely igneous or magmatic-hydrothermal magnetite. Childress et al. (2016) also report new $\delta^{18}\text{O}$ values for magnetite that range from $+1$ to $+4\text{‰}$, which are consistent with equilibration of magnetite with moderate to high temperature hydrothermal solutions.

The published $\delta^{18}\text{O}$ and $\delta^{56}\text{Fe}$ data, Zr-in-rutile and Ti-in-quartz thermometry data, and the trace element variability of Type 1, Type 2 and Type 3 magnetite, can be combined to discuss a plausible model for the genesis of the Pea Ridge magnetite ore body. Type 1 magnetite crystallized from a silicate melt. This is evident from the Ti-enriched composition of Type 1 magnetite as well as published stable Fe isotope data for magnetite from the same samples that were studied in this thesis. Type 1 magnetite subsequently re-equilibrated with high-temperature hydrothermal fluid, likely via dissolution-reprecipitation, consistent with the presence of rutile, which is known to form via exsolution of Ti from igneous Ti-rich phases during post-mineralization hydrothermal alteration in porphyry ore-forming systems (Scott, 2005; Rabbia et al., 2009). This high-temperature hydrothermal re-equilibration of magnetite could have occurred during the mineralizing event, or following mineralization. According to the magnetite-fluid suspension model presented by Knipping et al. (2015a), it is plausible that igneous magnetite crystals were the nucleation site for a magmatic-hydrothermal fluid that exsolved from silicate melt. The exsolved fluid can envelop magnetite crystals, and owing to the lower bulk density of the magnetite-fluid suspension relative to the parent magma, the suspension can ascend and evolve from the magma body during regional tension. During ascent, the magnetite-fluid suspension cools and decompresses, which results in decreasing concentrations of Ti, V, Al, Mn, Ca in magnetite that continuously re-equilibrates with the surrounding fluid. According to Knipping et al. (2015a), this can plausibly explain the Type 2 magnetite in the Pea Ridge ore body. Following emplacement in the volcanic host rocks at Pea Ridge, a second hydrothermal event pervasively dissolved and re-precipitated magnetite. This produced the Type 3 magnetite, which formed at lower temperature and as a result has the lowest concentrations of the trace elements Ti, V, Ca, Al and Mn.

Conclusion

The Pea Ridge deposit is one of the major iron oxide deposits is hosted in the St. Francois Mountain terrane in Missouri. The concentrations of the trace elements Ti, V, Ca, Al and Mn in magnetite indicate three different types of magnetite in the deposit. Type 1 is magmatic, Type 2 is high-temperature hydrothermal, and Type 3 is moderate temperature hydrothermal. There is a significant amount of scatter for the trace element concentrations of each of the three types of magnetite. However, the magnetite trace element compositions appear to vary systematically and correlate with temperatures determined by Ti-in-rutile and Ti-in-quartz thermometry. The variability of magnetite trace element chemistry, where magnetite grains plot in the igneous (Fe-Ti, V) field, the Kiruna field, the IOCG field, the BIF field, and the Skarn field, suggests that syn- and post-mineralization hydrothermal alteration makes the application of the discriminant diagram concept less than straightforward. The trace element data reported in this thesis, combined with published Fe and O isotope data, are consistent with the recently proposed magnetite-fluid suspension genetic model for the Pea Ridge magnetite deposit.

References

- Ayuso, R.A., Slack, J.F., Day, W.C., McCafferty, A.E., 2016. Geochemistry, Nd-Pb isotopes, and Pb-Pb ages of the Mesoproterozoic Pea Ridge iron oxide-apatite-rare earth element deposit, southeast Missouri, USA: *Economic Geology*.
- Barton, M.D., 2014. Iron Oxide (–Cu–Au–REE–P–Ag–U–Co) Systems: Treatise on Geochemistry (Second Edition). *Geochemistry of Mineral Deposits*, 13, 515-541.
- Barton, M. D., Johnson, D. A., 1996. Evaporitic-source model for igneous-related Fe oxide–(REE-Cu-Au-U) mineralization. *Geology*, 24, 259-262.
- Bickford, M. E., Mose, D. G., 1975. Geochronology of Precambrian Rocks in the St. Francois Mountains, South eastern Missouri. *Geological Society of America Special Papers*, 165, 1-48.
- Benavides, J., Kyser, T. K., Clark, A. H., Oates, C. J., Zamora, R., Tarnovschi, R., Castillo, B., 2007. The Mantoverde iron oxide-copper-gold district, III Región, Chile: the role of regionally derived, nonmagmatic fluids in chalcopyrite mineralization. *Economic Geology*, 102, 415-440.
- Buddington, A. F., Lindsley, D H., 1964. Iron-titanium oxide minerals and synthetic equivalents. *Journal of Petrology*, 5, 310-357.
- Childress, T.M., Simon, A.C., Day, W.C., Lundstrom, C.C., Bindeman, I.N., 2016. Iron and Oxygen isotope signatures of the Pea Ridge and Pilot Knob magnetite–apatite deposits, southeast Missouri, USA. *Journal of Economic Geology*, 111.
- Dare, S.A., Barnes, S.J., Beaudoin, G., Méric, J., Boutroy, E., Potvin-Doucet, C., 2014. Trace elements in magnetite as petrogenetic indicators. *Mineralium Deposita*, 49, 785-796.
- Dare, S. A., Barnes, S. J., Méric, J., Néron, A., Beaudoin, G., Boutroy, E., 2013. The use of trace elements in Fe-oxides as provenance and petrogenetic indicators in magmatic and hydrothermal environments. In: *Mineral Deposit Research for a High-Tech World. 12th SGA Biennial Meeting Proceedings*, 1, 256-259.
- Day, W. C., Slack, J. F., Ayuso, R. A., Seeger, C. M., 2016. Regional Geologic and Petrologic Framework for the Iron Oxide ± Apatite ± Rare Earth Element and Iron Oxide-Copper-Gold Deposits of the Mesoproterozoic St. Francois Mountains Terrane, Southeast Missouri, USA, *Economic Geology*, In print.
- Dupuis, C., 2009. Iron-oxide trace element fingerprinting of mineral deposit types. *Exploring for Iron Oxide Copper–Gold Deposits: Canada and Global Analogues, Short Course Volume. Geological Association of Canada Annual Meeting*, 107–121.
- Dupuis, C., Beaudoin, G., 2011. Discriminant diagrams for iron oxide trace element fingerprinting of mineral deposit types. *Mineralium Deposita*, 46, 319-335.

- Emery, J.A., 1968. Geology of the Pea Ridge iron orebody, in Ridge, J.D., ed, Ore deposits of the United States, 1933–1967, The Graton-Sales volume: New York, American Institute of Mining, Metallurgical, and Petroleum Engineers, I, 359–369.
- Fisher, L. A., Kendrick, M. A., 2008. Metamorphic fluid origins in the Osborne Fe oxide–Cu–Au deposit, Australia: Evidence from noble gases and halogens. *Mineralium Deposita*, 43, 483–497.
- Goldschmidt, V.M., 1954. *Geochemistry*: Oxford University Press, London, 730.
- Hoffman, P. F., 1989. Precambrian geology and tectonic history of North America. *The Geology of North America*, 447–512.
- Hu, H., Lentz, D., Li, J. W., McCarron, T., Zhao, X. F., Hall, D., 2015. Reequilibration processes in magnetite from iron skarn deposits. *Economic Geology*, 110, 1–8.
- Husman, J.R., 1989. Gold, rare earth element, and other potential by-products of the Pea Ridge iron ore mine. Missouri Department of Natural Resources, Contributions to Precambrian Geology, 21, Open File Report OFR-89-78-MR, 18.
- Johnson, C.A., Day, W.C, and Rye, R.O., 2016. Oxygen, hydrogen, sulfur, and carbon isotopes in the Pea Ridge magnetite-apatite deposit, southeast Missouri, and sulfur isotope comparisons to other iron deposits in the region. *Economic Geology*.
- Johnson, C.A., Day, W.C., and Rye, R.O., 2013. Stable isotope geochemistry of the Pea Ridge iron oxide-rare earth element deposit, St. Francois Mountains, southeastern Missouri: Temperature of ore formation, source of hydrothermal fluid, and source of sulfur. *Geological Society of America, Abstracts with Programs*, 45, 499.
- Jonsson, E., Troll, V. R., Högdahl, K., Harris, C., Weis, F., Nilsson, K. P., Skelton, A., 2013. Magmatic origin of giant ‘Kiruna-type’ apatite-iron-oxide ores in Central Sweden. *Scientific Reports*, 3. 1644–1652.
- King, E. M., Trzaskus, A. P., Valley, J. W., 2008. Oxygen isotope evidence for magmatic variability and multiple alteration events in the Proterozoic St. Francois Mountains, Missouri. *Precambrian Research*, 165, 49–60.
- Kisvarsanyi, E.B., 1981. Geology of the Precambrian St. Francois terrane, southeastern Missouri. Missouri Department of Natural Resources, Contribution to Precambrian Geology Report of Investigations, 64, 58.
- Kisvarsanyi, E.B., 1990. General features of the St. Francois and Spavinaw granite-rhyolite terranes and Precambrian metallogenic region of southeast Missouri. *United States Geological Survey Bulletin*, 1332, 48–57.
- Kisvarsanyi, G., Kisvarsanyi, E. B., 1989. Precambrian geology and ore deposits of the southeast Missouri iron metallogenic province. Olympic Dam-type deposits and geology of Middle Proterozoic rocks in the St. Francois Mountains terrain, Missouri. Edited by VM Brown,

- EB Kisvarsanyi and RD Hagni. Society of Economic Geologists Guidebook Series, 4, 1-40.
- Kisvarsanyi, E. B., Kisvarsanyi, G., 1990. Alkaline granite ring complexes and metallogeny in the Middle Proterozoic St. Francois terrane, southeastern Missouri, USA. Mid-Proterozoic Laurentia-Baltica: Geological Association of Canada Special Paper, 38, 433-446.
- Kisvarsanyi, G., Proctor, P.D., 1967. Trace element content of magnetites and hematites, southeast Missouri metallogenic province, U.S.A. *Economic Geology*, 62, 449–471.
- Knipping, J.L., Bilenker, L., Simon, A.C., Reich, M., Barra, F., Deditius, A., Lundstrom, C., Bindeman, I., Munizaga, R., 2015a. Giant Kiruna-type deposits form by efficient flotation of magmatic magnetite suspensions. *Geology*, 43, 591–594.
- Knipping, J.L., Bilenker, L., Simon, A.C., Reich, M., Barra, F., Deditius, A., Wälle, M., Heinrich, C.A., Holtz, F., Munizaga, R., 2015b. Trace elements in magnetite from massive iron oxide-apatite deposits indicate a combined formation by igneous and magmatic-hydrothermal processes. *Geochimica et Cosmochimica Acta*, 171, 15-38.
- Lindsley, D.H., 1976. The crystal chemistry and structure of oxide minerals as exemplified by the Fe–Ti oxides. *Oxide Minerals*, 3, L1–L60.
- Lindsley, D.H., 1991. Experimental studies of oxide minerals. *Review in Mineralogy and Geochemistry*, 25, 106.
- Marikos, M.A., Nuelle, L.M., Seeger, C.M., 1989. Geology of the Pea Ridge mine in Brown, M.V., Kisvarsanyi, E.B., and Hagni, R.D., eds., “Olympic Dam-type” deposits and geology of Middle Proterozoic rocks in the St. Francois Mountains terrane, Missouri. Society of Economic Geologists Guidebook Series, 4, 41–54.
- Marikos, M.A., Nuelle, L.M., Seeger C.M., 1990. Geologic mapping and evaluation of the Pea Ridge iron ore mine (Washington County, Missouri) for rare earth element and precious metals potential: A progress report. *United States Geological Survey Bulletin*, 1932, 76–81.
- McClenaghan, M.B., 2005. Indicator mineral methods in mineral exploration. *Geochemistry: Exploration Environmental Analysis*, 5, 233–245.
- Meighan, C.J., Hofstra, A.H., Marsh, E.E., Lowers, H.A., Koenig, A.E., Hitzman, M.W., 2015. Zr-in-rutile and Ti-in-quartz thermometry support a metasomatic origin for the Pea Ridge iron oxide-apatite-REE deposit, southeast Missouri, USA. Society of Economic Geologists Conference 2015, Hobart, Tasmania, Sept. 27–30, 2015, Abstracts Volume (CD).
- Menuge, J.F., Brewer, T.S., Seeger, C.M., 2002. Petrogenesis of metaluminous A-type rhyolites

- from the St. Francois Mountains, Missouri and the Mesoproterozoic evolution of the southern Laurentian margin. *Precambrian Research*, 113, 269–291.
- Mollo, S., Putirka, K., Iezzi, G., Scarlato, P., 2013. The control of cooling rate on titanomagnetite composition: Implications for a geospeedometry model applicable to alkaline rocks from Mt. Etna volcano. *Contribution to Mineralogy Petrology*, 165, 457–475.
- Nadoll, P., Mauk, J.L., Hayes, T.S., Koenig, A.E., Box, S.E., 2012. Geochemistry of magnetite from hydrothermal ore deposits and host rocks of the Mesoproterozoic Belt Supergroup, United States. *Economic Geology*, 107, 1275–1292.
- Nadoll, P., Mauk, J. L., Leveille, R. A., Koenig, A. E., 2015. Geochemistry of magnetite from porphyry Cu and skarn deposits in the southwestern United States. *Mineralium Deposita*, 50, 493-515.
- Nadoll, P., Angerer, T., Mauk, J. L., French, D., Walshe, J., 2014. The chemistry of hydrothermal magnetite: a review. *Ore Geology Reviews*, 61, 1-32.
- Nold, J.L., Davidson, P., Dudley, M.A., 2013. The Pilot Knob magnetite deposit in the Proterozoic St. Francois Mountains terrane, southeast Missouri, USA: A magmatic and hydrothermal replacement iron deposit. *Ore Geology Reviews*, 53, 446–469.
- Nold, J.L., Dudley, M.A., Davidson, P., 2014. The southeast Missouri (USA) Proterozoic iron metallogenic province: Types of deposits and genetic relationships to magnetite-apatite and iron oxide-copper-gold deposits. *Ore Geology Reviews*, 57, 154–171.
- Nuelle, L.M., Kisvarsanyi, E.B., Seeger, C.M., Day, W.C., Sidder, G.B., 1991. Structural setting and control of the Pea Ridge magnetite deposit, Middle Proterozoic St. Francois terrane, Missouri. *Geological Society of America, Abstracts with Programs*, 23, A292.
- Nuelle, L. M., Desborough, G. A., Hatch, J. R., Leventhal, J. S., 1992. Geology and Mineral Paragenesis of the Pea Ridge Iron Ore Mine, Washington County, Missouri-Origin of the Rare-earth-element-and Gold-bearing Breccia Pipes. *United States Geological Survey Bulletin*, 1989, p. A1-A11.
- Nyström, J.O., Billström, K., Henríquez, F., Fallick, A.E., Naslund, H.R., 2008, Oxygen isotope composition of magnetite in iron ores of the Kiruna type in Chile and Sweden: GFF [Geologiska Föreningen], 130, 177–188.
- Pollard, P. J., 2006. An intrusion-related origin for Cu–Au mineralization in iron oxide–copper–gold (IOCG) provinces. *Mineralium Deposita*, 41, 179-187.
- Rabbia, O.M., Hernández, L.B., French, D.H. et al., 2009. The El Teniente porphyry Cu–Mo deposit from a hydrothermal rutile perspective. *Miner Deposita*, 44, 849-866.
- Rieger, A. A., Marschik, R., Díaz, M., Hölzl, S., Chiaradia, M., Akker, B., & Spangenberg, J. E., 2010. The hypogene iron oxide copper-gold mineralization in the Mantoverde district, Northern Chile. *Economic Geology*, 105, 1271-1299.

- Rieger, A. A., Marschik, R., & Díaz, M., 2012. The evolution of the hydrothermal IOCG system in the Mantoverde district, northern Chile: new evidence from microthermometry and stable isotope geochemistry. *Mineralium Deposita*, 47, 359-369.
- Rivers, T., Corrigan, D., 2000. Convergent margin on southeastern Laurentia during the Mesoproterozoic: Tectonic implications. *Canadian Journal Earth Sciences*, 37, 359–383.
- Scott, Keith M., 2005. Rutile geochemistry as a guide to porphyry Cu–Au mineralization, Northparkes, New South Wales, Australia. *Geochemistry: Exploration, Environment, Analysis*, 5, 247-253.
- Seeger, C.M., Nuelle, L.M., Day, W.C., Sidder, G.B., Marikos, M.A., Smith, D.C., 2001. Geologic maps and cross sections of mine levels at the Pea Ridge iron mine, Washington County, Missouri. United States Geology Survey Field Studies Map, 2353, 6.
- Shannon, R. T., 1976. Revised effective ionic radii and systematic studies of interatomic distances in halides and chalcogenides. *Acta Crystallographica Section A: Crystal Physics, Diffraction, Theoretical and General Crystallography*, 32, 751-767.
- Sidder, G.B., Day, W.C., Nuelle, L.M., Seeger, C.M., Kisvarsanyi, E.B., 1993. Mineralogic and fluid-inclusion studies of the Pea Ridge iron-rare earth-element deposit, southeast Missouri. *United States Geology Survey Bulletin*, 2039, 205–216.
- Sillitoe, R.H., Burrows, D.R., 2002. New field evidence bearing on the origin of the El Laco magnetite deposit, northern Chile. *Economic Geology*, 97, 1101–1109.
- Toplis, MJ, Carroll MR., 1995. An experimental study of the influence of oxygen fugacity on Fe-Ti oxide stability, phase relations, and mineral-melt equilibria in ferro-basaltic systems. *Journal of Petrology*, 36, 1137-1170.
- Van Schmus, W. R., Bickford, M. E., Turek, A., 1996. Proterozoic geology of the east-central Midcontinent basement. *Special Papers: Geological Society of America*, 7-32.
- Walker, J.A., Pippin, C.G., Cameron, B.I., Patino, L., 2002. Tectonic insights provided by Mesoproterozoic mafic rocks of the St. Francois Mountains, southeastern Missouri. *Precambrian Research*, 117, 251–268.
- Wechsler, B.A., Lindsley, D.H., Prewitt, C.T., 1984. Crystal structure and cation distribution in titanomagnetites ($\text{Fe}_{3-x}\text{Ti}_x\text{O}_4$). *American Mineralogists*, 69, 754–770.
- Whitten, C.W., Yancey, R.J., 1990. Characterization of the rare-earth mineralogy at the Pea Ridge deposit, Missouri. *United States Bureau of Mines Report Investigations*, 9331, 9

Figures

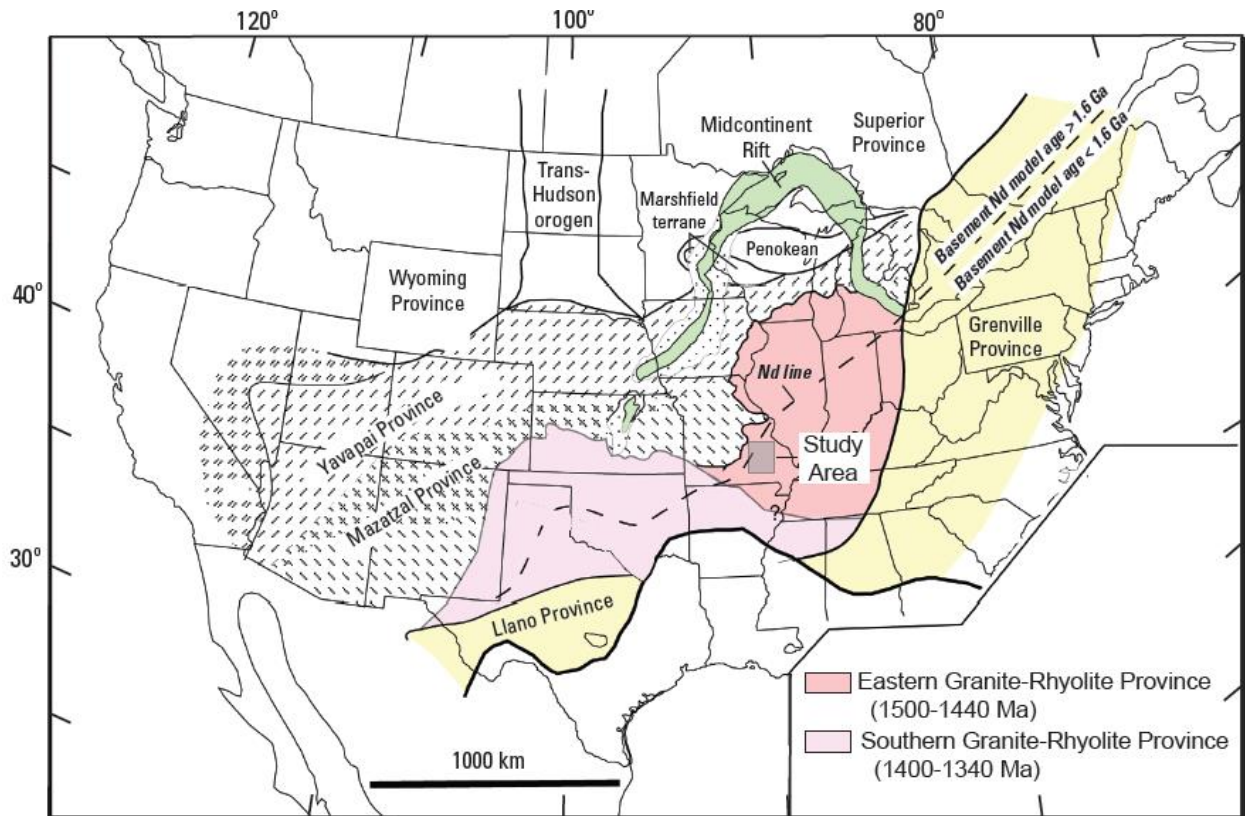


Figure 1. The geological provinces of North America. The study area is indicated with white box. Figure from Day et al. (2016).

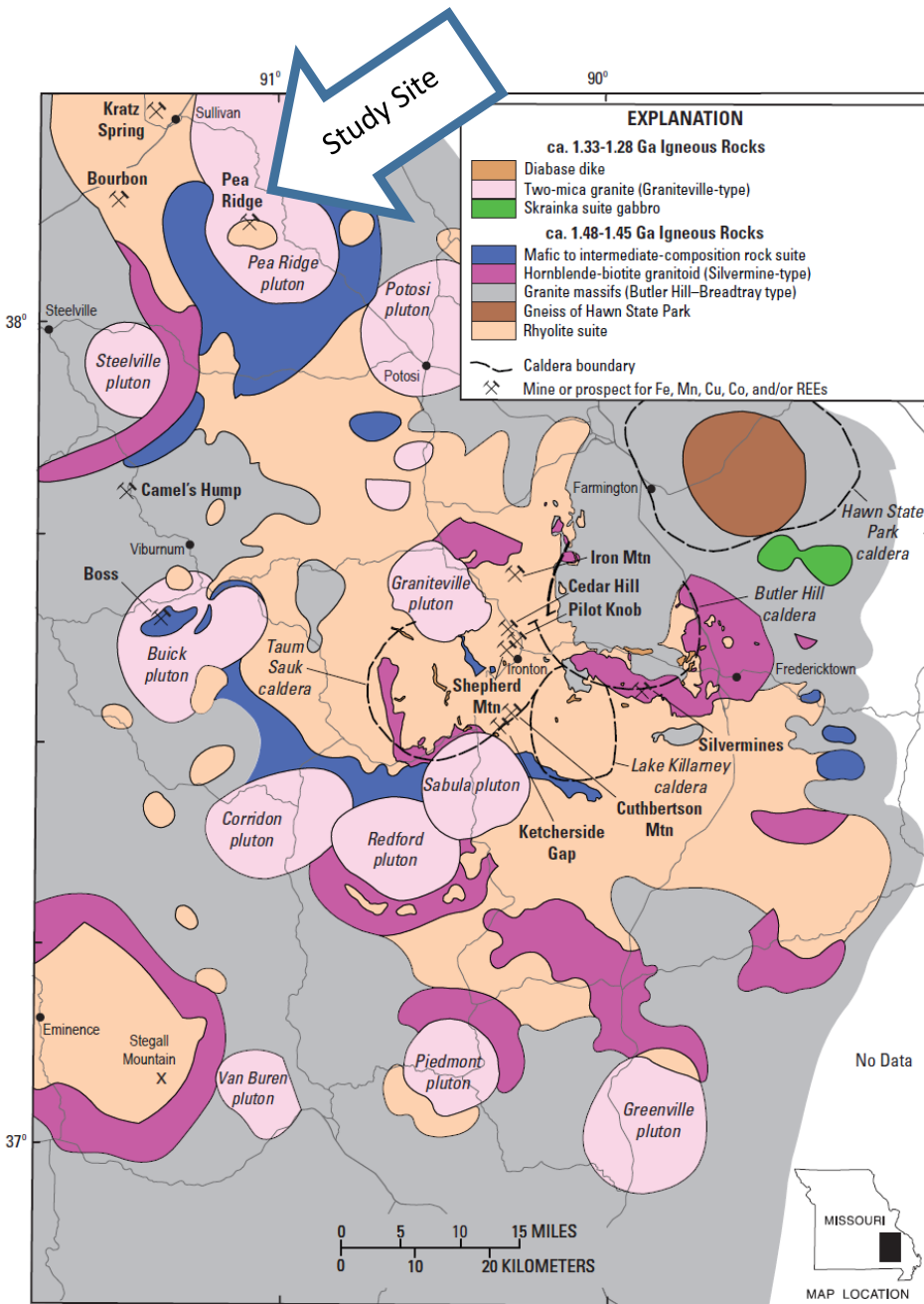


Figure 2. Geological map of the St. Francois Mountain terrane in southeast Missouri, U.S.A. showing iron-oxide deposits in bold writing. The white arrow indicates the study site. Modified from Day et al. (2016).

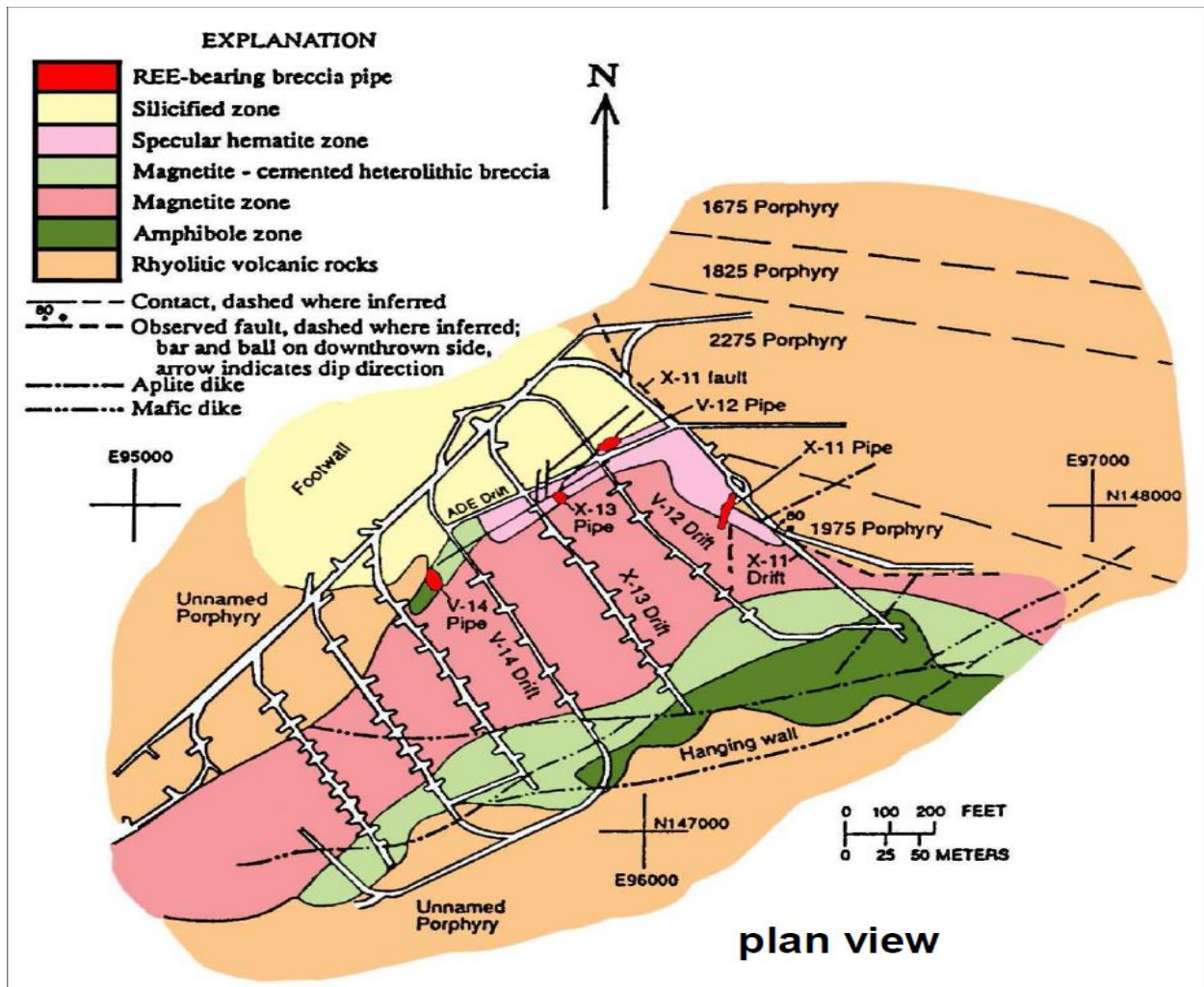


Figure 3. Structures and orientation of the Pea Ridge deposit hosted in rhyolitic volcanic rocks. This deposit is zoned vertically with a sequence of mineralization, outward from the massive magnetite to the iron-oxides cemented breccia. Figure from Seeger et al. (2001).

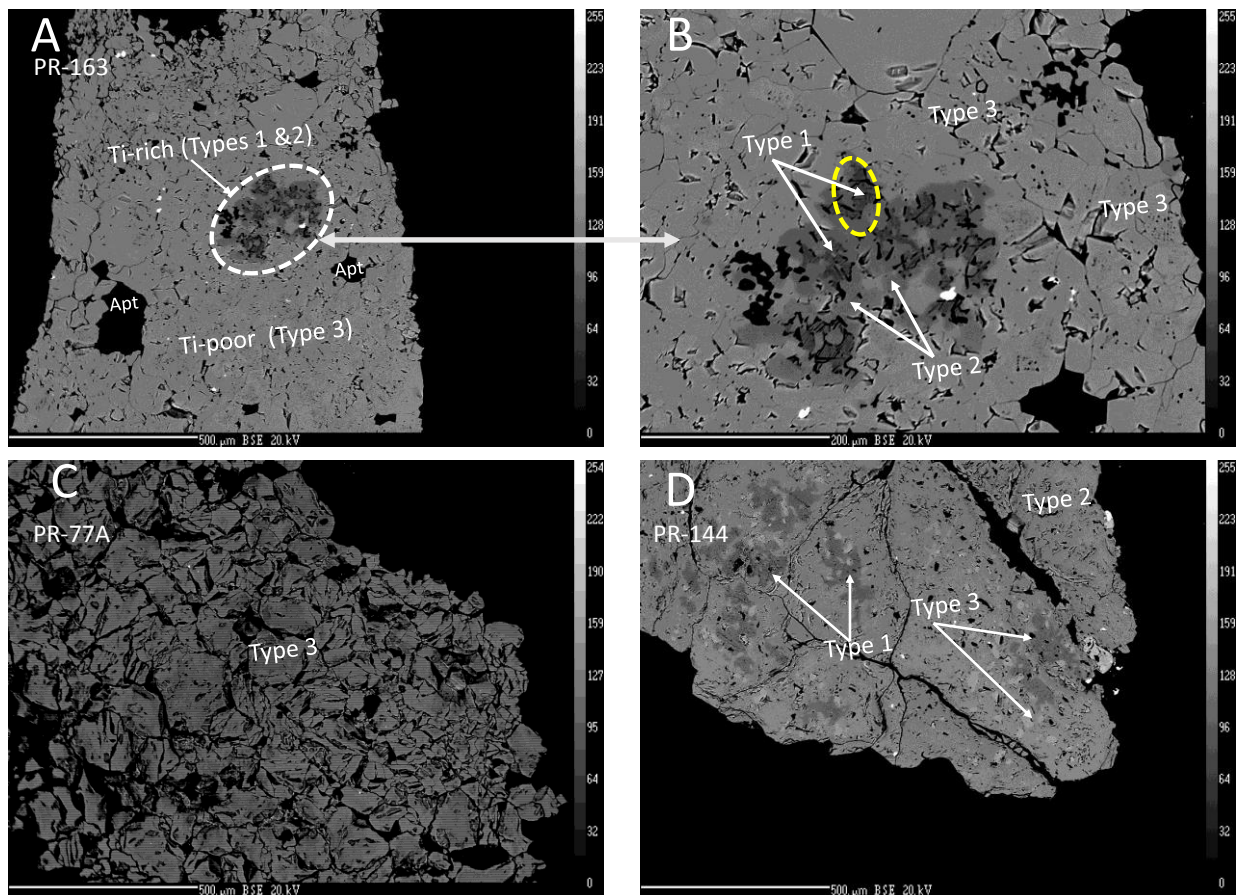


Figure 4. Backscattered electron (BSE) images reveal three types of magnetite generations in Pea Ridge. A) Sample PR-163 is Ti-rich magnetite (circled area) surrounded by Ti-poor magnetite. B) Zoomed-in section of panel A showing three compositionally distinct magnetite populations: Type 1 (dark gray), high Ti (avg. 8.4 wt. %), thought to be magmatic in origin and is characterized by exsolution lamellae of ilmenite; Type 2 (light gray), moderate Ti (Avg. 0.456 wt. %), thought to replace Type 1; then Type 3, depleted in Ti (<0.1 wt. %), thought to replace Type 2. C) Sample PR-77A shows only Type 3 magnetite, which is the modally dominant type in all samples analyzed. D) Sample PR-144 also reveals three types of magnetite, comparable to PR-163 in panel A. Scale bars are 500 microns in panels A, C, D, and 200 microns in panel B.

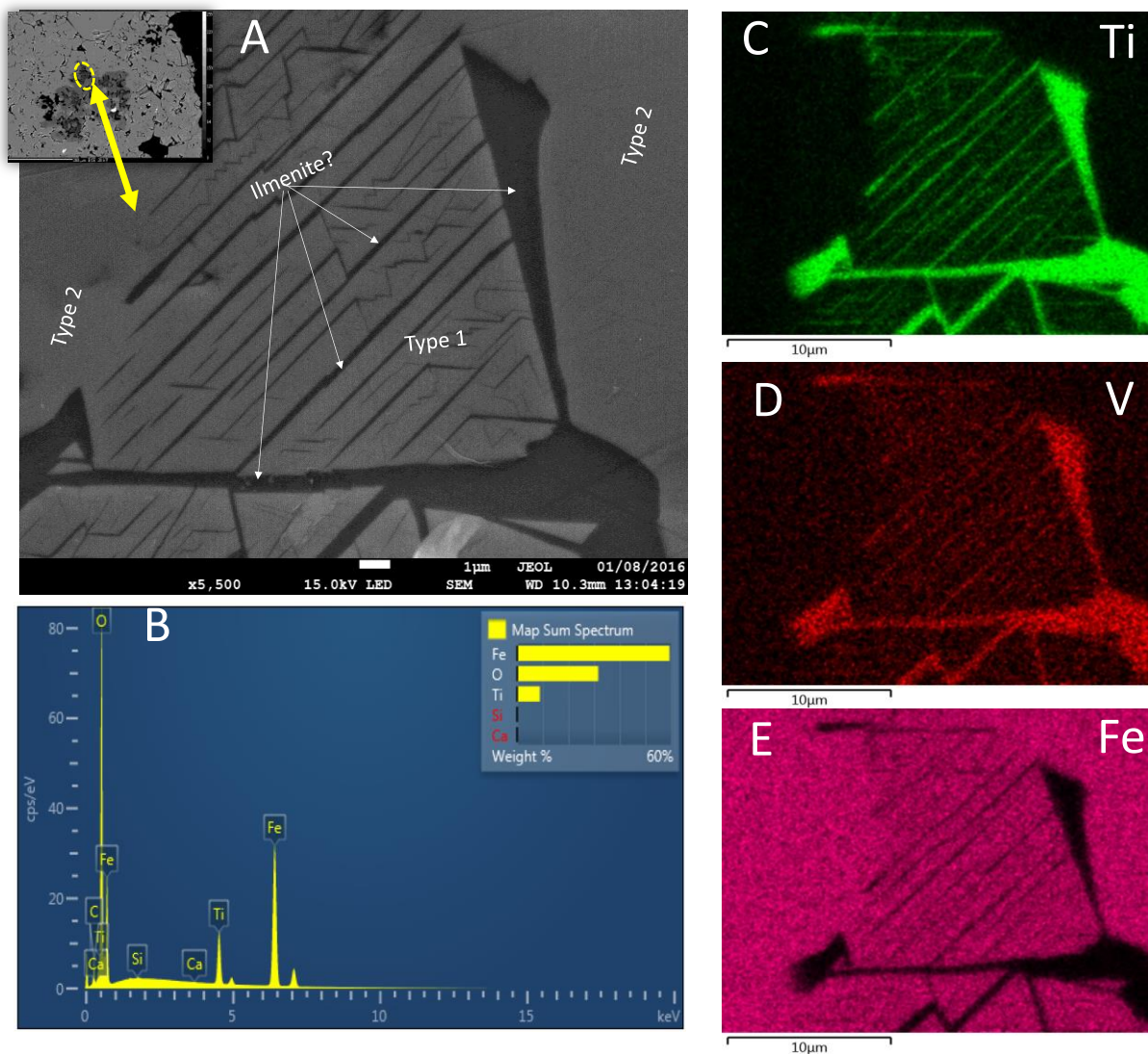


Figure 5. Energy dispersive X-ray spectrometry (EDS) elemental maps acquired from the Ti-rich Type 1 magnetite grains of sample PR-163. (A) Back scattered electron image showing the exsolved ilmenite lamellae. B) The EDS spectrum and elemental quantitative data of panel A. C, D and E show high resolution EDS maps of Ti, V and Fe, respectively.

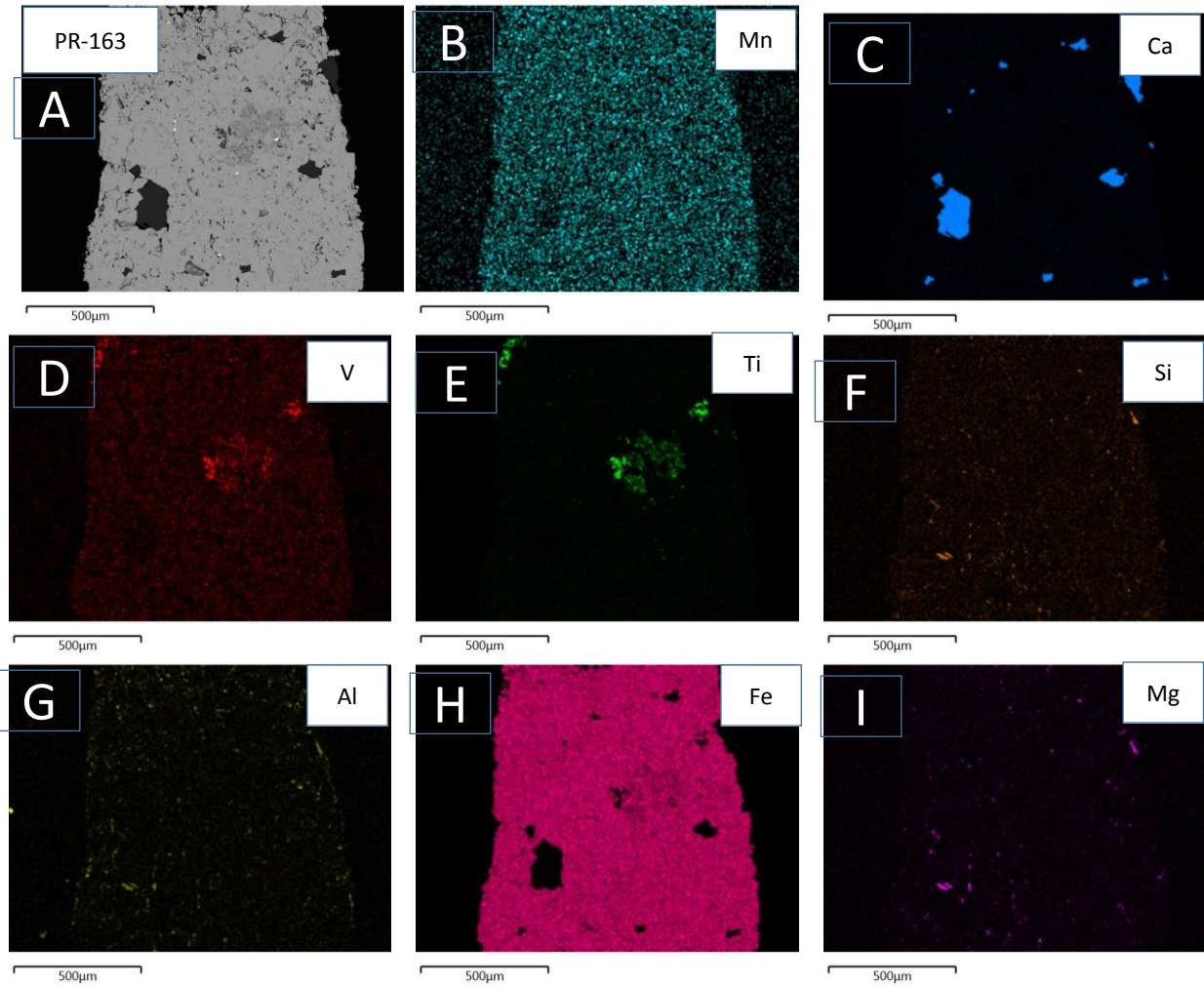


Figure 6. A) Back scattered electron image of magnetite grains from sample PR-163; and energy dispersive X-ray spectrometry (EDS) element maps of the same magnetite sample for: B) Manganese (Mn), C) Calcium (Ca), D) Vanadium (V), E) Titanium (Ti), F) Silicon, G) Aluminum (Al), H), Iron (Fe) and I) Magnesium (Mg).

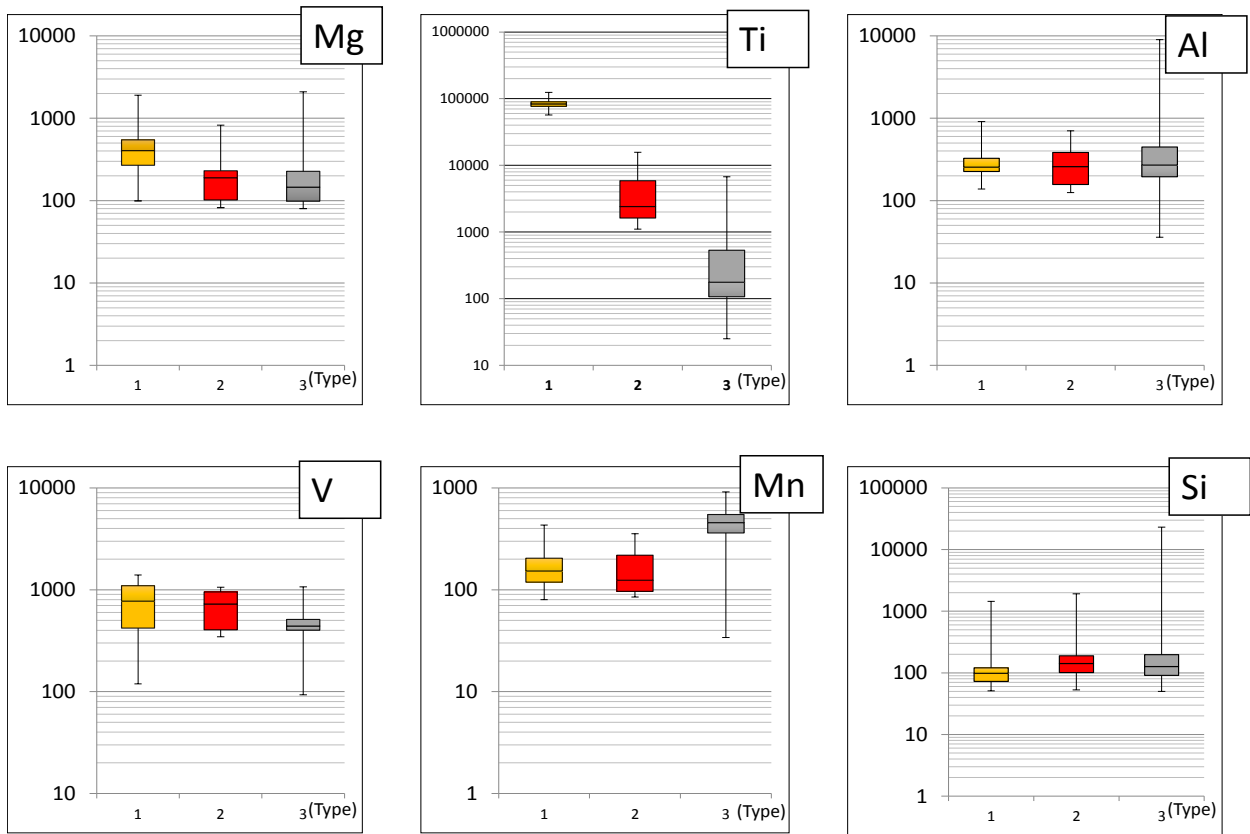


Figure 7. Box and whisker plots show variation in the compositions of Ti, V, Mg, Al, Si and Mn elements for the three types of magnetite in the Pea Ridge Deposit.

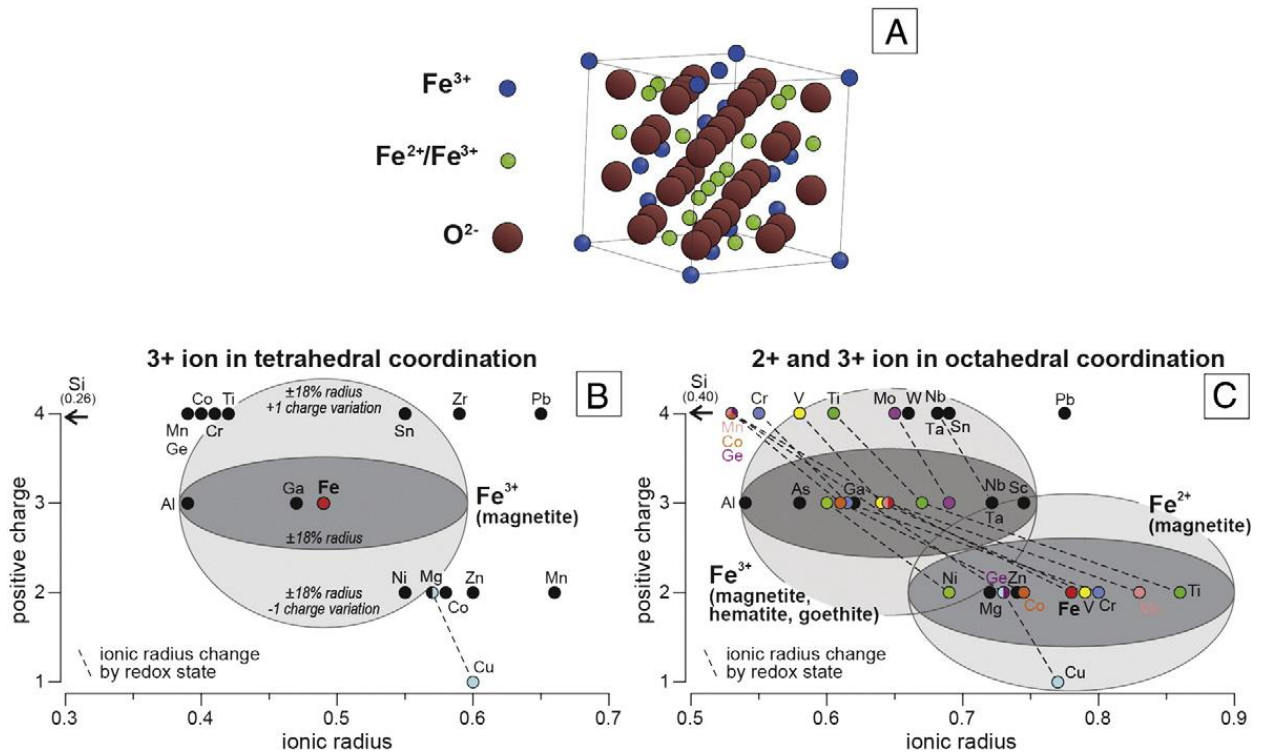


Figure 8. (A) The magnetite inverse spinel structure. (B) Charge vs ionic radius plots indicates trace elements that substitute into the tetrahedral ferric ion site of the magnetite inverse spinel structure; (C) Charge vs ionic radius plots indicates trace elements that substitute into the octahedral ferric/ferrous ion site of the magnetite inverse spinel structure; Some cations, e.g., Ti⁴⁺, require coupled substitution, which is controlled by temperature and oxygen fugacity (Lindsley, 1991). Taken from Nadoll et al. (2013) (with data from Shannon, 1976).

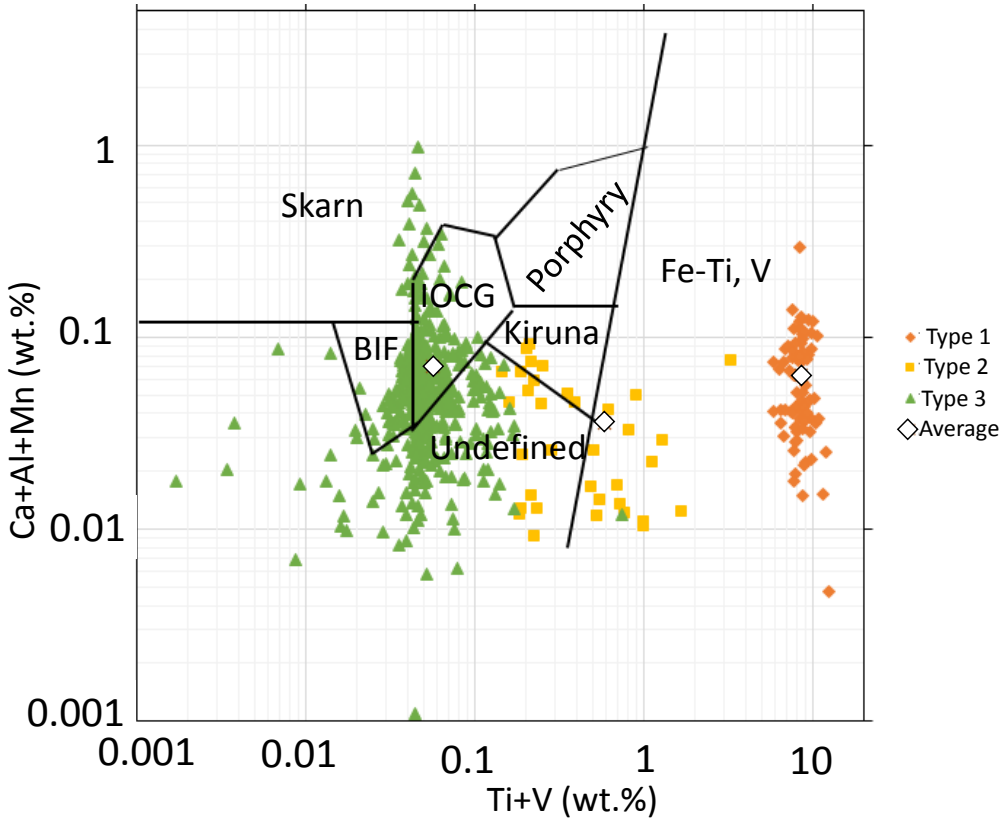


Figure 9. The $[Ca+Al+Mn]$ vs $[Ti+V]$ discriminant diagram (Dupuis and Beaudoin, 2011) that separates different deposit types based on the chemistry of magnetite and hematite. The Pea Ridge magnetite compositions fall in different fields. Type 1 falls in the high temperature magmatic (Fe-Ti, V) field; Types 2 and 3 spread across IOA-Kiruna, IOCG, BIF and Skarn fields, which are indicative of high and low temperature hydrothermal deposits. The average of each magnetite type is indicated by a diamond symbol.

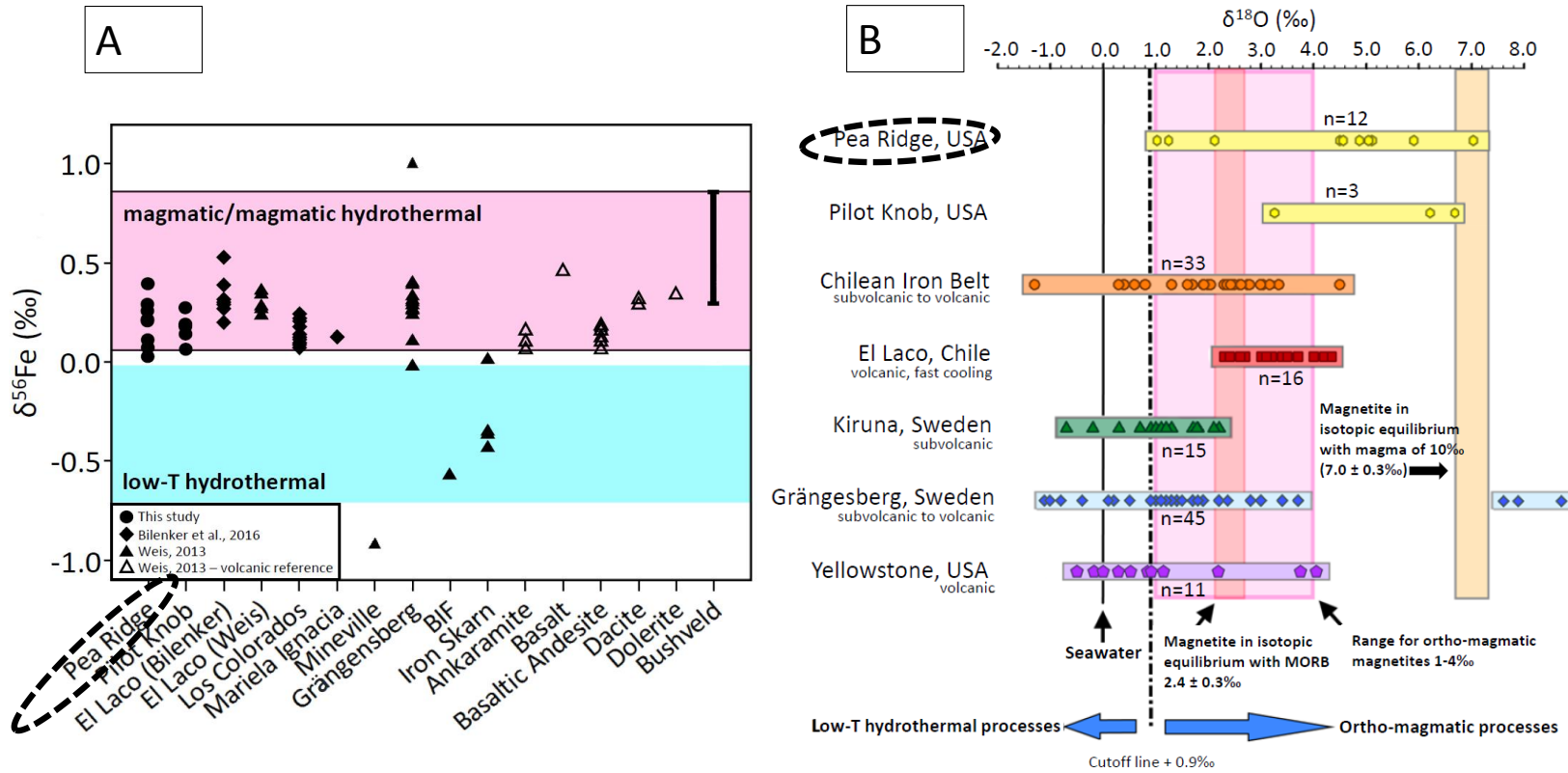


Figure 10. Published stable iron (A) and oxygen (B) isotope data for the same magnetite samples investigated in this thesis (Pea Ridge deposit; dashed ellipse) are consistent with all Fe and O in the deposit originating from a magmatic source reservoir.. Reproduced from Childress et al. (2016).

Tables

Table 1. Pea Ridge magnetite samples information provided by J. W. Slack and W.C Day from the United States Geological Survey (USGS), USA.

Collection	Deposit	Sample #	Latitude	Longitude	Core #	Depth (ft)	Rock type	Description	Mine level and Drift
Warren Day	Pea Ridge	PR-77A	38.123370	-91.050885	Not provided	Not provided	Massive magnetite ore	Magnetite-rich, 40' south of REE breccia pipes	2370;PDD-6
Warren Day	Pea Ridge	PR-82B	38.122524	-91.050264	Not provided	Not provided	Magnetite ore zone	Equigranular magnetite ore, with lots sulfides, with mt-ap-py clasts? In f.g. Magnetite-py matrix	2370;PDD-6
Warren Day (1992)	Pea Ridge	PR-144	38.122862	-91.050585	UD12-E	2440	Magnetite ore	Magnetite ore from core, magnetite py-(8%) with late ap-calcite-quartz (?), chip	2440; + UD12W-OP23
Warren Day	Pea Ridge	PR-148	38.123165	-91.048609	Not provided	Not provided	Massive ore	Foliated magnetite-hematite ore, Because see no tectonic foliation in any other units, must be flow foliation? Seams of late quartz-calcite. Apatite occurs in late vug.	2125;X11; 1124bx-cut; S.W. corner
Warren Day	Pea Ridge	PR-153	38.123657	-91.050296	Not provided	Not provided	Massive magnetite ore	Magnetite ore with interstitial quartz-apatite, mullions of fault surfaces cut massive silicified zone. Deformation=post-silicic phase.	2275; +ADE-V125
Warren Day (1992)	Pea Ridge	PR-73	38.123393	-91.050902	Underground	2370	Magnetite ore zone	Apatite -bearing magnetite ore	2370; + PDD-6
Warren Day (1992)	Pea Ridge	PR-82A	38.122524	-91.050264	Underground	Not provided	Magnetite ore zone	Clastic-fined grain magnetite ore, with lots of sulfides, mineral phase=magnetite + apatite + pyrite, magnetite-pyrite matrix	2370; PDD-6
Warren Day (1992)	Pea Ridge	PR-163	38.123832	-91.050449	Underground	2370	Massive ore	Massive magnetite-hematite ore, with disseminated seams and pods of ap-quartz; act inter-grown with magnetite	2370; AD;end
Warren Day	Pea Ridge	PR-65	Not provided	Not provided	Not provided	Not provided	Not provided	Not provided	Not provided
Warren Day	Pea Ridge	PR-37	Not provided	Not provided	Not provided	Not provided	Not provided	Not provided	Not provided
Warren Day	Pea Ridge	PR-64A	Not provided	Not provided	Not provided	Not provided	Not provided	Not provided	Not provided
Warren Day	Pea Ridge	PR-18	Not provided	Not provided	Not provided	Not provided	Not provided	Not provided	Not provided

Table 2. EPMA crystal standards and analytical conditions.

Element	Spectrometer	Crystal	Standard block	Counting time	Detection Limit (wt. %)
Si:Ka	1	LTAP	W011	100	0.005
Ti:Ka	4	LLIF	Geik	120	0.006
Al:Ka	5	TAP	JADE	100	0.013
Fe:Ka	3	LLIF	Magnetite	20	0.022
V:Ka	3	LLIF	V2O5	120	0.006
Cr:Ka	4	LLIF	C2O3	100	0.013
Mn: Ka	3	LLIF	BHRH	100	0.008
Ca:Ka	2	PET	WOLL	100	0.008
Mg:Ka	1	LTAP	GEIK	100	0.008

Table 3. Major and trace element chemistry of magnetite grains from the Pea Ridge iron oxide deposit. Concentrations are expressed in weight percent (wt. %). The averages and 1-sigma standard deviations (STD) for magnetite types 1, 2 and 3 are presented at the bottom of each table. Empty data boxes indicate that the concentration of the element was below the limit of detection.

Type 1 magnetite													
Sample	Mg	Al	Si	Ca	Ti	V	Cr	Mn	Fe	O	Total	Mn+Al+Ca	Ti+V
PR-144-dg-02	0.055	0.048	0.009		9.212	0.136		0.021	58.616	23.107	91.203	0.069	9.348
PR-144-dg-04	0.022	0.040			8.538	0.129		0.013	59.497	22.874	91.122	0.053	8.668
PR-144-dg-04	0.027	0.037	0.005		7.454	0.121		0.013	57.636	21.613	86.911	0.051	7.576
PR-144-dg-05	0.018	0.041	0.008		5.710	0.121		0.015	62.818	21.932	90.662	0.056	5.831
PR-144-dg-06	0.080	0.024			9.923	0.133		0.015	58.465	23.526	92.172	0.040	10.056
PR-144-dg-08	0.051	0.028			9.643	0.137			57.969	23.183	91.027	0.028	9.781
PR-144-dg-09	0.055	0.029			9.618	0.135		0.021	58.246	23.255	91.371	0.049	9.753
PR-144-dg-10	0.042	0.036	0.013		10.516	0.138		0.024	56.801	23.444	91.012	0.060	10.654
PR-144-dg-11	0.037	0.016			9.280	0.131		0.028	58.632	23.118	91.256	0.043	9.412
PR-144-dg-12	0.055	0.024	0.008		8.606	0.132		0.019	59.224	22.850	90.919	0.043	8.738
PR-144-dg-13	0.051	0.026			6.796	0.122		0.010	61.251	22.219	90.496	0.052	6.917
PR-144-dg-14	0.042	0.025	0.007		6.957	0.122		0.023	61.028	22.257	90.467	0.048	7.079
PR-144-dg-15	0.023	0.026	0.007		6.200	0.115		0.019	62.442	22.138	90.972	0.045	6.314
PR-144-dg-17	0.080	0.034	0.005		7.510	0.125		0.025	60.258	22.436	90.474	0.058	7.636
PR-144-dg-18	0.050	0.024	0.006		8.175	0.127		0.021	59.828	22.732	90.969	0.045	8.302
PR-144-dg-19	0.014	0.016	0.010		9.782	0.135			57.819	23.202	90.985	0.016	9.917

PR-144-dg-20	0.012	0.023	0.008	8.092	0.140	0.008	58.938	22.406	89.642	0.031	8.232
PR-144-dg-21	0.011	0.023	0.011	6.349	0.101	0.009	62.014	22.103	90.630	0.031	6.450
PR-144-dg1-04	0.060	0.042		7.638	0.074	0.008	60.983	22.682	91.473	0.050	7.711
PR-144-dg1-08	0.057	0.033		8.669	0.072	0.013	59.800	23.026	91.661	0.046	8.742
PR-144-g1-13	0.038	0.060		8.336	0.072	0.012	59.884	22.843	91.242	0.073	8.408
PR-144-dg1-20	0.014	0.021	0.008	10.142	0.075	0.013	57.571	23.332	91.157	0.034	10.216
PR-144-dg1-11	0.028	0.023		6.664	0.074	0.024	61.819	22.236	90.852	0.046	6.738
144a-dg-01	0.040	0.025	0.009	8.551	0.079	0.011	59.909	22.962	91.566	0.037	8.630
144a-dg-03	0.039	0.026	0.005	8.194	0.081	0.011	60.397	22.862	91.596	0.037	8.275
144a-dg-04	0.029	0.023	0.010	7.600	0.079	0.011	61.227	22.703	91.674	0.035	7.679
144a-dg-05	0.042	0.025	0.010	9.067	0.078	0.009	59.197	23.104	91.512	0.035	9.145
144a-dg-06	0.055	0.035	0.008	8.398	0.078	0.019	60.188	22.963	91.727	0.054	8.476
144a-dg-08	0.033	0.032	0.006	7.887	0.083	0.013	60.721	22.751	91.507	0.045	7.970
144a-dg-10	0.039	0.027	0.007	8.342	0.076	0.013	60.014	22.850	91.349	0.040	8.419
144a-dg-11	0.051	0.028	0.006	8.401	0.080	0.014	59.963	22.891	91.423	0.042	8.481
144a-dg-12	0.041	0.026	0.012	8.603	0.082	0.016	59.596	22.917	91.274	0.042	8.684
144a-dg-13	0.061	0.022	0.011	8.710	0.079	0.024	59.480	22.968	91.342	0.046	8.788
144a-dg-15	0.043	0.035	0.013	7.515	0.084	0.008	60.921	22.580	91.184	0.043	7.599
144a-dg-16	0.037	0.036	0.012	7.802	0.082	0.020	60.509	22.645	91.125	0.056	7.884
144a-dg-17	0.010	0.020	0.011	6.746	0.085	0.011	61.977	22.336	91.186	0.032	6.831
144a-dg-18	0.019	0.037	0.011	8.322	0.079	0.022	60.298	22.931	91.709	0.060	8.401
144a-dg-19	0.190	0.087	0.145	8.221	0.067	0.018	60.322	23.170	92.207	0.104	8.288
144a-dg-20	0.028	0.028	0.011	7.151	0.082	0.011	61.267	22.419	90.982	0.039	7.233
144a-dg-21	0.071	0.033	0.012	8.333	0.068	0.017	60.077	22.900	91.500	0.050	8.401

144a-dg-22	0.022	0.023	0.011	9.503	0.073		58.823	23.277	91.722	0.023	9.576
144a-dg-23	0.022	0.018	0.009	7.972	0.077	0.012	60.453	22.720	91.272	0.029	8.048
PR-144a-dg-1	0.053		0.014	8.998	0.067	0.018	58.809	22.701	90.387	0.018	9.065
PR-144a-dg-2	0.068		0.014	7.286	0.072	0.036	61.052	22.208	90.454	0.036	7.358
PR-144a-dg-3	0.079		0.012	8.225	0.073	0.043	59.847	22.498	90.493	0.043	8.298
PR-144a-dg-4	0.073		0.012	7.810	0.070	0.025	59.909	22.225	89.838	0.025	7.880
PR-144a-dg-5	0.070		0.025	8.763	0.068	0.018	58.947	22.605	90.221	0.018	8.831
PR-144a-dg-6	0.039		0.030	7.734	0.075	0.014	60.419	22.324	90.357	0.014	7.809
PR-144a-dg-7	0.064		0.020	7.628	0.066	0.015	60.686	22.316	90.498	0.015	7.694
PR-144ay-01	0.061	0.026	0.010	8.534	0.034	0.020	59.586	22.868	91.136	0.046	8.568
PR-144ay-02	0.047	0.025	0.009	10.445	0.023	0.010	57.467	23.521	91.552	0.036	10.469
PR-144ay-03	0.052	0.024	0.010	8.379	0.037	0.019	59.698	22.790	91.008	0.042	8.417
PR-144ay-04	0.107	0.091	0.009	8.557	0.024	0.036	59.264	22.878	90.964	0.127	8.581
PR-144ay-05	0.041	0.024	0.011	9.317	0.026	0.015	58.681	23.113	91.227	0.038	9.344
PR-144by-07	0.042	0.051	0.045	8.164	0.033	0.011	59.836	22.739	90.920	0.062	8.196
PR-144cy-07	0.051	0.029	0.007	8.294	0.027	0.009	59.714	22.731	90.861	0.038	8.322
PR-144cy-08	0.032	0.025	0.007	8.870	0.032	0.012	58.664	22.807	90.457	0.037	8.901
PR-144cy-010	0.025	0.022	0.008	7.934	0.036		60.241	22.625	90.902	0.022	7.970
PR-144cy-012 line	0.024	0.027	0.008	6.667	0.048		61.311	22.093	90.184	0.027	6.714
PR-144cy-012 line	0.025	0.021	0.014	10.743	0.012	0.017	56.693	23.480	91.002	0.038	10.755
PR-144cy-012 line	0.044	0.023	0.010	9.235	0.024	0.023	58.411	22.985	90.759	0.046	9.259
PR-144cy-49	0.030	0.014	0.007	9.547	0.018	0.018	58.263	23.128	91.032	0.032	9.566
PR-144cy-50	0.027	0.027	0.007	7.878	0.037	0.014	60.295	22.612	90.904	0.041	7.915
PR-144cy-51	0.024	0.022	0.011	7.950	0.034	0.010	60.504	22.713	91.272	0.032	7.984

PR-144cy-53	0.028	0.019	0.012	6.365	0.047	0.017	62.314	22.183	90.988	0.036	6.412
PR-144cy-55	0.024	0.020	0.008	7.852	0.035	0.014	60.097	22.528	90.580	0.034	7.888
PR-144cy-56	0.112	0.017	0.006	9.039	0.027	0.040	59.321	23.155	91.719	0.057	9.066
PR-144cy-57	0.058	0.031	0.008	8.678	0.031	0.021	58.895	22.766	90.489	0.051	8.709
PR-144cy-59	0.027	0.032	0.007	8.821	0.030	0.011	58.989	22.866	90.785	0.043	8.851
PR-144cy-60	0.033	0.018	0.007	7.862	0.033	0.016	60.379	22.617	90.965	0.034	7.895
PR-144cy-61	0.033	0.023	0.006	8.875	0.031	0.013	59.195	22.954	91.125	0.036	8.905
PR-163d-dg-1	0.010		0.010	9.650	0.110	0.023	57.220	22.797	89.686	0.023	9.760
PR-163d-dg-2			0.015	12.448	0.072		55.638	24.045	91.928	0.000	12.520
PR-163d-dg-3			0.012	8.555	0.104	0.014	59.874	22.669	90.933	0.014	8.659
PR-163d-dg-4			0.017	7.609	0.113	0.024	60.802	22.316	90.587	0.024	7.722
PR-163d-dg-5			0.008	11.489	0.105	0.011	55.072	23.264	89.672	0.011	11.594
PR-163d-dg-6			0.010	11.827	0.100	0.021	55.485	23.611	90.777	0.021	11.926
PR-163d-dg-2		0.025		5.741	0.115	0.015	63.566	22.135	91.607	0.041	5.856
PR-163d-dg-3		0.022		7.380	0.115	0.018	60.892	22.464	90.906	0.041	7.496
PR-163b-dg-2		0.024		8.541	0.109	0.010	59.670	22.880	91.237	0.034	8.650
PR-163b-dg-3		0.026	0.045	9.193	0.112	0.014	59.021	23.182	91.595	0.040	9.305
Average	0.044	0.029	0.013	8.420	0.079	0.017	59.649	22.776	90.970	0.041	8.499
STD	0.027	0.013	0.018	1.243	0.036	0.007	1.563	0.423	0.694	0.018	1.241

Type 2 magnetite	Mg	Al	Si	Ca	Ti	V	Cr	Mn	Fe	O	Total	Mn+Al+Ca	Ti+V
------------------	----	----	----	----	----	---	----	----	----	---	-------	----------	------

Sample											
PR-144-wg-04			0.008	0.190	0.043		72.207	20.851	93.309	0.000	0.233
PR-144-wg-06	0.019	0.016	0.071	0.183	0.043	0.024	72.212	20.948	93.514	0.040	0.226
PR-144-wg-11		0.016	0.019	0.241	0.044		71.710	20.768	92.813	0.016	0.285
PR-144-wg1-06		0.027	0.015	0.167	0.043	0.026	72.401	20.924	93.604	0.052	0.210
PR-144-wg1-11			0.011	0.177	0.042	0.011	72.500	20.928	93.669	0.011	0.219
PR-144-wg1-13	0.017	0.015	0.010	0.111	0.035	0.034	72.430	20.894	93.548	0.049	0.146
144a-wg-01	0.024	0.020	0.019	0.152	0.037	0.021	71.886	20.783	92.949	0.041	0.189
144a-wg-03	0.008	0.014	0.016	0.348	0.043	0.023	71.143	20.683	92.283	0.037	0.390
144a-wg-06	0.019	0.037	0.023	0.175	0.036	0.036	71.630	20.742	92.702	0.072	0.211
144a-wg-07	0.044	0.024	0.014	0.161	0.042	0.020	71.847	20.783	92.935	0.043	0.203
PR-144a-wg-6			0.016	0.143	0.083		69.505	19.795	89.250	0.000	0.226
PR-163d-lg-1	0.010		1.979	0.413	0.081	0.012	67.730	21.707	91.627	0.012	0.494
PR-163d-lg-2			0.013	0.905	0.098		69.295	20.245	90.261	0.000	1.003
PR-163d-lg-3			0.014	1.569	0.102		68.548	20.491	90.444	0.000	1.670
PR-163d-lg-4			0.015	0.681	0.095	0.009	69.287	20.081	89.851	0.009	0.776
PR-163d-lg-5			0.009	0.893	0.106	0.009	68.551	20.008	89.252	0.009	0.999
PR-163d-lg-6	0.083		0.078	0.627	0.097	0.009	69.052	20.152	89.833	0.009	0.724
PR-37dg-19		0.059	0.029	0.163	0.054	0.015	69.440	20.120	89.883	0.074	0.217
PR-144by-09		0.037	0.010	0.254	0.103		69.625	20.212	90.252	0.037	0.357
PR-144cy-09	0.043	0.070	0.192	0.219	0.036		68.581	20.123	89.266	0.070	0.256
PR-144cz-21			0.011	0.150	0.040	0.011	72.114	20.793	93.117	0.011	0.190
PR-144cz-27		0.013	0.017	0.157	0.036	0.012	72.042	20.797	93.077	0.025	0.193
PR-144cz-30	0.010	0.037	0.047	0.121	0.041	0.009	71.928	20.806	93.004	0.046	0.162

PR-144cz-31			0.012		0.150	0.035		71.936	20.755	92.911		0.184
PR-144cx-43		0.045	0.008		0.209	0.038		69.640	20.164	90.113	0.045	0.247
PR-73bx-09		0.013	0.013		0.476	0.080		69.093	20.183	89.868	0.013	0.556
PR-73dz-017		0.029			1.204	0.094		68.516	20.508	90.352	0.029	1.297
PR-73dz-018		0.020			1.037	0.092		68.512	20.391	90.058	0.020	1.129
PR-73dz-019		0.046	0.017		0.837	0.072		68.902	20.396	90.276	0.046	0.909
PR-73dz-020			0.006		0.426	0.100		69.507	20.255	90.296		0.527
PR-73dz-021		0.017	0.010		0.608	0.096		69.108	20.274	90.106	0.017	0.703
PR-65ax-03		0.042	0.017		0.526	0.091		67.715	19.846	88.229	0.042	0.616
PR-65ax-05		0.025	0.007		0.412	0.095		69.380	20.224	90.139	0.025	0.506
PR-65ax-014		0.030	0.005		0.732	0.089		68.903	20.307	90.072	0.030	0.821
PR-163dc1	0.018		0.045		0.553	0.058	0.063	72.111	21.151	94.027	0.063	0.611
PR-163dc2			0.029		0.591	0.051	0.052	72.273	21.186	94.212	0.052	0.642
PR-163dc3			0.036		0.585	0.060	0.063	72.237	21.197	94.215	0.063	0.644
PR-163dc5			0.035		0.038	0.064	0.049	72.417	20.869	93.496	0.049	0.102
PR-163dc6	0.047	0.014	0.883		0.151	0.063	0.064	71.713	21.754	94.710	0.079	0.214
PR-163dc7			0.027		0.097	0.056	0.046	72.510	20.912	93.662	0.046	0.153
PR-163dc8	0.008		0.041		0.154	0.067	0.057	72.350	20.954	93.676	0.057	0.221
PR-163dc10			0.045		0.703	0.057	0.061	72.201	21.265	94.358	0.061	0.760
PR-163dc11	0.033	0.026	0.532		0.098	0.051	0.058	70.250	20.899	91.984	0.084	0.149
PR-163dc12	0.026	0.017	0.066		0.212	0.057	0.054	72.128	20.974	93.575	0.071	0.269
PR-163dc19			0.014		0.561	0.095	0.012	69.860	20.468	91.035	0.012	0.656
PR-163dc20			0.011		0.590	0.084	0.010	70.231	20.586	91.541	0.010	0.675
PR-163dc26		0.039	0.033		0.769	0.080	0.028	70.662	20.881	92.503	0.067	0.850

PR-163dc27	0.023	0.021	0.649	0.069	0.030	71.266	20.947	93.030	0.053	0.718	
PR-163dc28		0.033	0.519	0.067	0.044	71.530	20.940	93.162	0.044	0.585	
PR-163dc30		0.045	0.575	0.055	0.049	72.290	21.202	94.248	0.049	0.630	
PR-163d-gray6		0.010	0.755	0.096	0.009	69.868	20.592	91.353	0.009	0.851	
PR-163d-gray7	0.015	0.011	0.038	0.407	0.069	0.026	70.034	20.449	91.071	0.037	0.477
PR-163d-gray11		0.017	0.755	0.092		69.876	20.600	91.366	0.000	0.847	
PR-163d-gray12		0.012	0.629	0.093	0.012	69.969	20.535	91.268	0.012	0.721	
PR-163d-gray13		0.027	0.607	0.091		70.023	20.549	91.322	0.000	0.697	
PR-163d-gray14	0.011		0.025	0.599	0.092	0.010	69.998	20.536	91.273	0.010	0.691
PR-163d-gray15		0.031	0.502	0.079	0.027	70.601	20.655	91.918	0.027	0.581	
PR-163d-gray16		0.011	0.807	0.085	0.014	69.870	20.628	91.437	0.014	0.891	
PR-163d-gray17	0.009		0.022	0.881	0.086	0.011	69.737	20.657	91.433	0.011	0.967
PR-163d-gray19	0.014		0.036	0.409	0.069	0.040	71.715	20.923	93.229	0.040	0.478
PR-163d-gray20	0.018		0.050	0.166	0.063	0.055	72.501	21.007	93.881	0.055	0.229
PR-163d-gray21	0.017	0.011	0.028	0.852	0.098	0.008	69.369	20.555	90.962	0.019	0.950
PR-163d-gray28	0.011		0.038	0.837	0.065	0.045	71.641	21.190	93.848	0.045	0.902
PR-163d-gray29		0.271	0.034	0.789	0.071	0.036	70.292	21.000	92.515	0.307	0.861
PR-163c-contact-2	0.008	0.013	0.053	0.475	0.062	0.043	71.344	20.888	92.914	0.056	0.537
PR-163c-contact-3	0.093	0.955	0.128	0.306	0.044	0.043	69.459	21.208	92.270	0.998	0.350
PR-163c-contact-4		0.025	0.033	0.323	0.063	0.057	72.138	21.005	93.678	0.082	0.386
PR-163c-contact-5	0.021	0.015	0.042	0.750	0.053	0.051	71.866	21.219	94.050	0.066	0.803
PR-163c-contact-7	0.011	0.150	0.036	0.305	0.056	0.058	72.028	21.076	93.746	0.207	0.360
PR-163d-contact 1	0.017		0.040	0.249	0.062	0.049	72.481	21.042	93.962	0.049	0.311
PR-163d-contact 2	0.008	0.011	0.040	0.219	0.064	0.051	72.466	21.020	93.897	0.062	0.282

PR-163d-contact 3	0.010		0.042	0.288	0.068	0.049	72.282	21.012	93.770	0.049	0.356
PR-163d-contact 7			0.238	0.485	0.090	0.009	69.754	20.633	91.229	0.009	0.575
PR-144a dark-line3	0.013	0.151	0.093	0.554	0.055		67.477	19.992	88.372	0.151	0.609
PR-144a dark-line4	0.070		0.099	0.367	0.032	0.010	66.868	19.599	87.083	0.010	0.399
PR-144a dark-line5	0.031	0.061	0.063	0.110	0.028		68.834	19.957	89.090	0.061	0.138
PR-144a dark-line6		0.089	0.027	0.043	0.069	0.012	69.166	19.998	89.419	0.102	0.112
PR-144a dark-line8		0.045	0.016		0.098	0.011	70.132	20.208	90.526	0.056	0.098
Average	0.024	0.064	0.078	0.456	0.068	0.031	70.573	20.665	91.887	0.057	0.518
STD	0.021	0.151	0.249	0.300	0.022	0.019	1.509	0.427	1.772	0.118	0.317

Type 3 magnetite													
Sample	Mg	Al	Si	Ca	Ti	V	Cr	Mn	Fe	O	Total	Mn+Al+Ca	Ti+V
PR-144-wg-03	0.022	0.029	0.042			0.044		0.015	72.454	20.873	93.483	0.066	0.044
PR-144-wg-05		0.014	0.015		0.066	0.048		0.054	72.238	20.806	93.242	0.068	0.114
PR-144-wg-07		0.021	0.017			0.040		0.042	72.250	20.773	93.149	0.064	0.040
PR-144-wg-08		0.022	0.012		0.099	0.049		0.043	71.199	20.534	91.959	0.065	0.148
PR-144-wg-09		0.034	0.038		0.009	0.045			72.535	20.882	93.541	0.034	0.054
PR-144-wg-10		0.019	0.012		0.020	0.053			72.297	20.776	93.158	0.019	0.073
PR-144-wg-13	0.019		0.008		0.070	0.039		0.027	72.032	20.739	92.939	0.045	0.109
PR-144-wg-15	0.009	0.061	0.014		0.013	0.035		0.039	72.258	20.820	93.255	0.109	0.048
PR-144-wg-16	0.020	0.024	0.037			0.041		0.024	72.208	20.792	93.149	0.068	0.041
PR-144-wg-17			0.024		0.008	0.042		0.025	72.186	20.752	93.048	0.025	0.050
PR-144-wg-18			0.008		0.008	0.045		0.028	72.655	20.873	93.632	0.028	0.053
PR-144-wg-19			0.010			0.046		0.028	72.298	20.784	93.210	0.028	0.046
PR-144-wg1-16		0.015	0.020			0.043		0.040	72.009	20.699	92.824	0.055	0.043
PR-144-g1-17	0.009	0.017	0.009		0.080	0.047		0.016	72.472	20.873	93.521	0.041	0.128
PR-144-wg1-07		0.021	0.022			0.040		0.047	72.422	20.836	93.404	0.069	0.040
144a-wg-02			0.013		0.076	0.043		0.036	72.219	20.798	93.198	0.036	0.119
144a-wg-05	0.011	0.036	0.015		0.084	0.041		0.032	72.292	20.849	93.360	0.078	0.125
144a-wg-08			0.016		0.014	0.040		0.030	72.264	20.770	93.147	0.030	0.054
144a-wg-09			0.017		0.003	0.046		0.036	72.497	20.830	93.432	0.036	0.049
144a-wg-10			0.013			0.040		0.016	72.602	20.850	93.537	0.016	0.040
144a-wg-11			0.014			0.041		0.029	72.422	20.801	93.314	0.029	0.041

144a-wg-12			0.018		0.044	0.028	72.356	20.788	93.241	0.028	0.044		
144a-wg-13			0.015		0.044	0.025	72.571	20.854	93.528	0.025	0.044		
144a-wg-14			0.020		0.043	0.031	72.365	20.812	93.307	0.031	0.043		
144a-wg-15			0.024		0.043	0.032	72.374	20.797	93.271	0.032	0.043		
144a-wg-16		0.030	0.016		0.094	0.076	69.716	20.124	90.065	0.034	0.170		
144a-wg-17			0.015			0.047	72.631	20.871	93.618	0.038	0.047		
144a-wg-18		0.013	0.015		0.013	0.051	72.167	20.744	93.033	0.057	0.051		
144a-wg-19			0.267		0.018	0.010	0.051	0.031	71.560	20.804	92.746	0.298	0.061
144a-wg-20		0.010	0.143		0.026		0.041	0.036	71.562	20.706	92.542	0.189	0.041
144a-wg-21		0.008	0.019		0.015		0.038	0.044	72.069	20.714	92.901	0.072	0.038
PR-144a-wg-1			0.026		0.076	0.037			69.759	19.805	89.405	0.011	0.114
PR-144a-wg-2		0.010	0.026		0.075	0.032	0.040	0.040	72.249	20.532	92.659	0.040	0.107
PR-144a-wg-3		0.009	0.025		0.100	0.030	0.038	0.038	72.236	20.540	92.668	0.038	0.130
PR-144a-wg-4			0.016		0.673	0.070			69.291	20.082	89.838	0.000	0.743
PR-144a-wg-5			0.014		0.042	0.035			70.092	19.862	89.742	0.000	0.076
PR-163d-wg-1		0.011	0.046		0.036	0.062	0.050	0.050	72.011	20.483	92.400	0.059	0.099
PR-163d-wg-2			0.031			0.057	0.058	0.058	72.004	20.443	92.323	0.101	0.057
PR-163d-wg-3		0.015	1.308		0.043	0.059	0.057	0.057	70.402	21.473	93.060	0.057	0.101
PR-163d-wg-4			0.022			0.060	0.061	0.061	72.225	20.480	92.536	0.061	0.060
PR-163d-wg-5		0.010	0.032			0.058	0.059	0.059	72.039	20.433	92.307	0.059	0.058
PR-163d-wg-6			0.025			0.063	0.061	0.061	72.390	20.524	92.739	0.061	0.063
PR-163d-wg-7			0.018			0.062	0.055	0.055	72.422	20.523	92.758	0.055	0.062
PR-163d-wg-8			0.020			0.062	0.056	0.056	73.093	20.720	93.634	0.066	0.062
PR-163d-wg-9			0.021			0.061	0.057	0.057	71.894	20.375	92.086	0.066	0.061

PR-163d-wg-10		0.063	0.063	0.057	72.008	20.449	92.308	0.057	0.063
PR-163d-wg-11		0.013	0.061	0.057	71.858	20.358	92.029	0.057	0.061
PR-163d-wg-12		0.017	0.063	0.053	71.778	20.336	91.924	0.064	0.063
PR-82Ad-wg-1		0.013	0.041	0.056	72.122	20.419	92.329	0.075	0.041
PR-82Ad-wg-2		0.048	0.041	0.060	71.994	20.433	92.263	0.069	0.041
PR-82Ad-wg-3		0.066	0.037	0.039	69.343	19.768	89.099	0.177	0.037
PR-82Ad-wg-4	0.010	0.114	0.038	0.034	69.437	19.801	89.153	0.049	0.038
PR-82Ad-wg-5		0.009	0.042	0.061	72.465	20.517	92.771	0.069	0.042
PR-82Ad-wg-6		0.018	0.039	0.062	72.425	20.525	92.760	0.074	0.039
PR-82Ad-wg-7		0.013	0.039	0.061	72.319	20.479	92.587	0.061	0.039
PR-82Ad-wg-8		0.014	0.038	0.064	72.479	20.528	92.801	0.064	0.038
PR-82Ad-wg-9		0.103	0.044	0.056	69.452	19.780	89.132	0.056	0.044
PR-82Ad-wg-10		0.352	0.041	0.036	68.965	19.934	89.048	0.047	0.041
PR-82Ad-wg-11	0.023	2.312	0.037	0.058	68.382	22.050	92.611	0.058	0.037
PR-82Ad-wg-12		0.020	0.036	0.047	70.169	19.857	89.792	0.047	0.036
PR-82Ad-wg-13		0.016	0.040	0.057	72.379	20.678	93.049	0.057	0.040
PR-82Ba-wg-1	0.014	0.007	0.052	0.047	72.610	20.850	93.566	0.061	0.052
PR-82Ba-wg-2		0.012	0.052	0.051	72.499	20.831	93.457	0.051	0.052
PR-82Ba-wg-3	0.017	0.012	0.049	0.050	72.375	20.797	93.296	0.067	0.049
PR-82Ba-wg-4		0.013	0.055	0.050	72.921	20.947	93.986	0.050	0.055
PR-82Ba-wg-5		0.007	0.049	0.047	72.696	20.877	93.682	0.047	0.049
PR-82Ba-wg-6	0.017		0.050	0.048	72.619	20.835	93.542	0.065	0.050
PR-82Ba-wg-7		0.011	0.051	0.045	72.527	20.837	93.485	0.045	0.051
PR-82Ba-wg-8	0.102	0.009	0.052	0.049	71.175	20.511	91.874	0.161	0.052

PR-18d-wg-1			0.029		0.040	0.056	70.687	20.039	90.541	0.066	0.040
PR-18d-wg-2	0.013		0.053		0.045	0.059	69.507	20.018	89.693	0.059	0.045
PR-18d-wg-3			0.021		0.044	0.057	69.889	19.846	89.594	0.057	0.044
PR-18d-wg-4			0.028		0.043	0.049	70.734	20.049	90.591	0.049	0.043
PR-18d-wg-5			0.041		0.043	0.056	69.300	19.664	88.799	0.056	0.043
PR-18d-wg-6			0.023		0.040	0.059	69.736	19.748	89.279	0.067	0.040
PR-37wg-1		0.031	0.016		0.041	0.046	72.469	20.844	93.452	0.078	0.041
PR-37wg-2		0.027	0.011		0.041	0.061	72.378	20.814	93.338	0.089	0.041
PR-37wg-3		0.034	0.010		0.042	0.063	72.122	20.747	93.026	0.098	0.042
PR-37wg-4		0.019	0.014		0.040	0.057	72.374	20.810	93.324	0.077	0.040
PR-37wg-5		0.025	0.018		0.040	0.050	72.059	20.722	92.916	0.075	0.040
PR-37wg-6		0.025	0.015		0.043	0.060	72.117	20.741	93.004	0.084	0.043
PR-37wg-7		0.028	0.014		0.041	0.058	72.679	20.902	93.725	0.086	0.041
PR-37wg-8	0.016	0.042	0.079		0.042	0.065	71.047	20.532	91.822	0.108	0.042
PR-37wg-9		0.040	0.012		0.044	0.060	72.340	20.817	93.320	0.100	0.044
PR-37wg-10	0.161	0.178	0.110		0.038	0.061	71.726	20.977	93.256	0.239	0.038
PR-37wg-11		0.028	0.015		0.043	0.060	72.515	20.861	93.532	0.088	0.043
PR-37wg-12		0.029	0.012		0.041	0.054	71.694	20.618	92.452	0.082	0.041
PR-37wg-13		0.034	0.010		0.042	0.061	72.144	20.754	93.054	0.095	0.042
PR-37wg-14	0.033	0.099	0.025		0.043	0.066	72.221	20.871	93.362	0.165	0.043
PR-37wg-15	0.040	0.313	0.035		0.042	0.055	71.326	20.819	92.636	0.368	0.042
PR-37wg-16		0.023	0.013		0.042	0.066	72.081	20.732	92.967	0.089	0.042
PR-37wg-17	0.050	0.103	0.030		0.041	0.071	71.981	20.823	93.102	0.174	0.041
PR-37wg-18	0.010	0.036	0.010		0.045	0.079	72.231	20.792	93.209	0.115	0.045

PR-37wg-19		0.029	0.011		0.039	0.058	72.560	20.864	93.564	0.087	0.039
PR-37wg-20		0.153	0.008		0.045	0.061	72.668	21.008	93.949	0.214	0.045
PR-37wg-21		0.024	0.011		0.044	0.060	71.826	20.653	92.622	0.085	0.044
PR-37wg-22	0.015	0.051	0.014		0.041	0.062	71.649	20.651	92.519	0.146	0.041
PR-37wg-23		0.024	0.009		0.043	0.060	71.903	20.671	92.711	0.083	0.043
PR-37wg-24		0.024	0.016		0.041	0.068	71.690	20.663	92.611	0.190	0.041
PR-37wg-25	0.014	0.093	0.024		0.040	0.074	71.720	20.728	92.723	0.167	0.040
PR-37wg-26		0.024	0.010		0.044	0.062	72.077	20.725	92.947	0.086	0.044
PR-37wg-27		0.031	0.013		0.043	0.062	72.030	20.722	92.908	0.092	0.043
PR-37wg-28		0.018	0.014		0.040	0.052	71.758	20.628	92.515	0.070	0.040
PR-37wg-29		0.025	0.009		0.038	0.056	71.938	20.683	92.759	0.081	0.038
PR-37wg-30		0.024	0.011		0.039	0.057	72.347	20.801	93.287	0.081	0.039
PRb-37wg-1		0.026	0.015		0.041	0.060	72.293	20.795	93.240	0.085	0.041
PRb-37wg-2		0.017	0.010		0.040	0.062	72.229	20.764	93.132	0.079	0.040
PRb-37wg-3		0.021	0.052		0.042	0.058	72.240	20.816	93.234	0.079	0.042
PRb-37wg-4		0.018	0.022		0.042	0.059	72.304	20.798	93.250	0.077	0.042
PRb-37wg-5		0.020	0.013		0.042	0.058	72.154	20.746	93.040	0.078	0.042
PRb-37wg-6	0.019	0.135	0.031		0.041	0.048	71.714	20.753	92.754	0.190	0.041
PRb-37wg-7		0.047	0.013		0.039	0.063	72.122	20.765	93.062	0.110	0.039
PRb-37wg-8		0.661	0.013		0.041	0.052	71.361	21.089	93.228	0.713	0.041
PRb-37wg-9		0.020	0.013	0.008	0.042	0.059	72.345	20.806	93.301	0.079	0.050
PRb-37wg-10		0.021	0.052		0.041	0.059	72.236	20.814	93.230	0.080	0.041
PR-153c-wg-1			0.014		0.041	0.042	72.633	20.862	93.599	0.042	0.041
PR-153c-wg-2			0.010		0.045	0.043	72.659	20.863	93.623	0.043	0.045

PR-153c-wg-3	0.017			0.043	0.039	72.710	20.870	93.667	0.056	0.043
PR-153c-wg-4		0.007		0.043	0.048	72.887	20.923	93.907	0.048	0.043
PR-153c-wg-5		0.016		0.043	0.040	72.322	20.773	93.200	0.040	0.043
PR-77Aa-wg-1	0.016	0.015		0.051	0.051	72.600	20.868	93.603	0.067	0.051
PR-77Aa-wg-2	0.018	0.016	0.010	0.052	0.048	72.399	20.824	93.375	0.066	0.062
PR-77Aa-wg-3	0.021	0.016		0.051	0.051	72.543	20.862	93.553	0.072	0.051
PR-77Aa-wg-4	0.025	0.005		0.051	0.045	72.932	20.953	94.002	0.071	0.051
PR-77Aa-wg-5	0.028	0.008		0.053	0.049	72.876	20.947	93.956	0.077	0.053
PR-77Aa-wg-6	0.014			0.050	0.051	72.767	20.904	93.804	0.085	0.050
PR-77Aa-wg-7	0.018	0.011		0.047	0.046	72.662	20.889	93.690	0.076	0.047
PR-148a-wg-1	0.036	0.013		0.036	0.017	72.465	20.822	93.382	0.053	0.036
PR-148a-wg-2	0.023	0.014		0.034	0.013	72.619	20.853	93.546	0.035	0.034
PR-148a-wg-3	0.020	0.016		0.034	0.013	72.534	20.833	93.447	0.033	0.034
PR-148a-wg-4	0.018	0.017		0.034	0.013	72.225	20.745	93.051	0.031	0.034
PR-148a-wg-5	0.030	0.015		0.036	0.013	72.919	20.950	93.957	0.043	0.036
PR-148a-wg-6	0.022	0.011		0.036	0.016	72.770	20.898	93.753	0.038	0.036
PR-148a-wg-7	0.025	0.009		0.034	0.012	72.691	20.880	93.664	0.053	0.034
PR-65c-wg-1		0.013		0.047	0.060	72.396	20.794	93.310	0.060	0.047
PR-65c-wg-2		0.010		0.044	0.075	72.187	20.739	93.063	0.075	0.044
PR-65c-wg-3		0.015		0.045	0.062	72.121	20.719	92.963	0.062	0.045
PR-65c-wg-4		0.013		0.045	0.056	72.245	20.756	93.129	0.056	0.045
PR-65c-wg-5		0.012		0.045	0.060	72.223	20.756	93.117	0.060	0.045
PR-144-lg-01	0.074	0.008	0.013	0.073		70.006	20.175	90.344	0.074	0.086
PR-144-lg-02		0.010	0.011			69.441	19.923	89.394	0.000	0.011

PR-144-lg-03		0.018	0.006		0.011	69.671	19.981	89.671	0.018	0.011	
PR-144-lg-04		0.032	0.012	0.025	0.055	69.734	20.077	89.957	0.032	0.080	
PR-144-lg-05		0.033	0.008		0.070	0.009	69.581	20.015	89.721	0.042	0.070
PR-144-lg-06		0.019	0.006	0.012	0.013	70.150	20.133	90.327	0.019	0.025	
PR-144-lg-07		0.043	0.010		0.026	69.737	20.039	89.849	0.043	0.026	
PR-144-lg-08		0.046	0.005	0.017	0.057	69.418	19.970	89.504	0.046	0.073	
PR-144-lg-09		0.033	0.009		0.020	69.774	20.034	89.855	0.033	0.020	
PR-144-lg-10		0.027	0.010	0.011	0.029	69.578	19.993	89.646	0.027	0.040	
PR-144-lg-11		0.048	0.025	0.017	0.080	69.677	20.093	89.951	0.048	0.098	
PR-144-lg-12		0.059	0.007		0.062	70.086	20.171	90.382	0.059	0.062	
PR-144-lg-13		0.050	0.006		0.019	70.105	20.150	90.330	0.050	0.019	
PR-144-lg-14	0.066	0.052	0.038		0.061	69.987	20.212	90.414	0.117	0.061	
PR-144-lg-16		0.117	0.006		0.051	69.840	20.141	90.144	0.117	0.051	
PR-144-lg-17		0.019	0.006		0.014	69.680	20.001	89.743	0.019	0.014	
PR-144-lg-18		0.027	0.007	0.009	0.034	69.413	19.936	89.419	0.027	0.044	
PR-144-lg-19		0.077	0.009	0.015	0.092	69.322	19.997	89.520	0.077	0.108	
PR-144-lg-20		0.017	0.009		0.009	70.101	20.111	90.241	0.017	0.009	
PR-144-lg1-01		0.034			0.041	70.145	20.147	90.365	0.034	0.041	
PR-144-lg1-05		0.027			0.023	70.192	20.145	90.387	0.027	0.023	
PR-144-lg1-10		0.027	0.014		0.024	69.944	20.091	90.101	0.027	0.024	
PR-144-lg1-12		0.085				70.559	20.289	90.932	0.085	0.000	
PR-144-lg1-16		0.014			0.027	70.261	20.144	90.428	0.014	0.027	
PR-144-lg1-20		0.029			0.025	70.244	20.161	90.457	0.029	0.025	
144a-lg-01			0.011	0.010	0.029	70.255	20.162	90.470	0.000	0.039	

144a-lg-02		0.020	0.011	0.009	0.057	70.194	20.172	90.462	0.020	0.066
144a-lg-03		0.025	0.012	0.019	0.054	70.156	20.174	90.437	0.025	0.073
144a-lg-04		0.024	0.005		0.046	70.395	20.215	90.684	0.024	0.046
144a-lg-05		0.013	0.007		0.048	70.346	20.192	90.603	0.013	0.048
144a-lg-06		0.019	0.008		0.039	70.377	20.204	90.646	0.019	0.039
144a-lg-07		0.020			0.042	70.365	20.196	90.625	0.020	0.042
144a-lg-08		0.033	0.009	0.019	0.046	70.209	20.183	90.493	0.033	0.065
144a-lg-09		0.016	0.011		0.039	70.165	20.145	90.378	0.016	0.039
144a-lg-10		0.046	0.011		0.051	70.158	20.174	90.438	0.046	0.051
144a-lg-11	0.008	0.071	0.007		0.010	70.139	20.173	90.410	0.079	0.010
144a-lg-12		0.048			0.061	70.076	20.146	90.325	0.048	0.061
144a-lg-13			0.007		0.029	70.330	20.168	90.529	0.000	0.029
144a-lg-14		0.045	0.008		0.077	69.953	20.117	90.189	0.045	0.077
144a-lg-15		0.017	0.009		0.045	70.129	20.128	90.317	0.017	0.045
144a-lg-16		0.023	0.006		0.049	70.129	20.133	90.331	0.023	0.049
144a-lg-17		0.023	0.007		0.043	70.094	20.122	90.284	0.023	0.043
144a-lg-18		0.029	0.008		0.054	70.015	20.116	90.223	0.029	0.054
144a-lg-19		0.018	0.010		0.042	70.264	20.173	90.507	0.018	0.042
PR-144a-lg-1			0.013		0.016	69.988	19.781	89.479	0.000	0.016
PR-144a-lg-2			0.013		0.042	70.078	19.840	89.678	0.004	0.042
PR-144a-lg-3			0.016		0.046	69.901	19.818	89.509	0.009	0.046
PR-144a-lg-4			0.021		0.037	69.578	19.705	89.047	0.009	0.037
PR-82Ad-lg-1			0.069		0.037	69.591	19.801	89.269	0.049	0.037
PR-82Ad-lg-2			0.041		0.042	69.614	19.742	89.170	0.053	0.042

PR-82Ad-Ig-3			0.010		0.039	0.053	69.584	19.694	89.063	0.053	0.039
PR-82Ad-Ig-4			0.010		0.038	0.053	69.894	19.772	89.435	0.053	0.038
PR-82Ad-Ig-5	0.009	0.444	0.200		0.040	0.051	68.067	20.169	88.996	0.509	0.040
PR-82Ad-Ig-6			0.042		0.045	0.039	69.375	19.673	88.863	0.054	0.045
PR-82Ad-Ig-7			0.038		0.039	0.054	69.698	19.766	89.291	0.073	0.039
PR-82Ad-Ig-8			0.206		0.037	0.052	69.570	20.188	90.050	0.066	0.037
PR-82Ba-Ig-1			0.011		0.053	0.052	72.195	20.740	93.053	0.052	0.053
PR-82Ba-Ig-2		0.013	0.014		0.056	0.055	72.349	20.794	93.279	0.068	0.056
PR-82Ba-Ig-3			0.016		0.054	0.053	72.229	20.760	93.125	0.053	0.054
PR-82Ba-Ig-4			0.017		0.050	0.051	72.017	20.699	92.846	0.051	0.050
PR-82Ba-Ig-5		0.031	0.028	0.052	0.053	0.067	72.366	20.876	93.483	0.098	0.105
PR-82Ba-Ig-6			0.015		0.054	0.053	72.723	20.897	93.749	0.053	0.054
PR-82Ba-Ig-7		0.013	0.015		0.054	0.055	72.646	20.876	93.649	0.068	0.054
PR-82Ba-Ig-8			0.022		0.053	0.051	72.328	20.785	93.237	0.051	0.053
PR-64Adc-Ig-1			0.016		0.047	0.028	68.963	19.525	88.264	0.028	0.047
PR-64dc-Ig2			0.023		0.043	0.034	69.591	19.798	89.269	0.034	0.043
PR-64dc-Ig3			0.038		0.048	0.027	69.462	19.720	89.015	0.027	0.048
PR-64dc-Ig4			0.044		0.045	0.029	69.532	19.743	89.112	0.029	0.045
PR-64dc-Ig5			0.020		0.050	0.042	72.949	20.677	93.426	0.042	0.050
PR-64dc-Ig6			0.014		0.050	0.034	71.623	20.280	91.682	0.042	0.050
PR-64dc-Ig8			0.017		0.051	0.039	71.897	20.360	92.038	0.039	0.051
PR-64dc-Ig9			0.020		0.051	0.036	72.364	20.504	92.659	0.036	0.051
PR-64A-Ig-10	0.031		0.044		0.050	0.036	72.185	20.514	92.563	0.045	0.050
PR-18-Ig-1			0.025		0.040	0.059	68.544	19.685	88.336	0.071	0.040

PR-18-1g-2			0.028		0.041	0.043	69.220	19.608	88.623	0.054	0.041
PR-18-1g-3			0.047		0.044	0.042	69.316	19.678	88.832	0.052	0.044
PR-18-1g-4			0.020		0.043	0.042	69.636	19.718	89.144	0.052	0.043
PR-18-1g-5			0.025	0.011	0.043	0.042	69.659	19.746	89.221	0.053	0.055
PR-18-1g-6			0.024		0.041	0.062	69.966	19.825	89.600	0.066	0.041
PRc-371g-1		0.062	0.015		0.042	0.062	72.203	20.798	93.184	0.124	0.042
PRc-371g-2	0.014	0.034	0.032		0.045	0.049	71.911	20.716	92.806	0.084	0.045
PRc-371g-3	0.020	0.038	0.026		0.042	0.066	72.294	20.831	93.323	0.103	0.042
PRc-371g-4	0.015	0.026	0.014		0.043	0.063	71.791	20.657	92.610	0.089	0.043
PRc-371g-5		0.072	0.013		0.043	0.051	72.513	20.896	93.598	0.124	0.043
PRc-371g-6	0.010	0.023	0.017		0.041	0.061	71.447	20.555	92.159	0.084	0.041
PRc-371g-7		0.035	0.017		0.039	0.051	72.006	20.720	92.878	0.086	0.039
PRc-371g-8	0.012	0.242	0.031		0.042	0.070	71.957	20.919	93.281	0.312	0.042
PRc-371g-9		0.025	0.011		0.044	0.062	72.140	20.747	93.038	0.086	0.044
PRc-371g-10		0.138	0.015		0.042	0.055	72.204	20.866	93.326	0.192	0.042
PRc-371g-11		0.025	0.009		0.044	0.064	72.446	20.835	93.433	0.089	0.044
PRc-371g-12		0.038	0.020		0.040	0.046	72.030	20.726	92.900	0.084	0.040
PRc-371g-13	0.010	0.020	0.010		0.039	0.058	72.125	20.736	92.998	0.078	0.039
PRc-371g-14		0.207	0.011		0.040	0.063	71.653	20.767	92.747	0.270	0.040
PRc-371g-15		0.032	0.018		0.043	0.049	71.912	20.694	92.758	0.081	0.043
PRc-371g-16	0.010	0.025	0.012		0.041	0.053	72.157	20.753	93.056	0.077	0.041
PRc-371g-17		0.026	0.014		0.040	0.063	72.493	20.850	93.494	0.088	0.040
PRc-371g-18		0.018	0.011		0.041	0.060	71.753	20.627	92.518	0.079	0.041
PRc-371g-19	0.070	0.898	0.026		0.042	0.075	71.622	21.439	94.178	0.973	0.042

PRc-37lg-20		0.022	0.011		0.041	0.061	72.347	20.799	93.285	0.083	0.041
PRc-37lg-21		0.034	0.010		0.037	0.057	72.233	20.776	93.156	0.091	0.037
PRc-37lg-22		0.417	0.015		0.043	0.063	71.750	20.990	93.291	0.480	0.043
PRc-37lg-23	0.012	0.014	0.013		0.043	0.053	71.677	20.608	92.426	0.067	0.043
PRc-37lg-24			0.009		0.041	0.057	72.379	20.796	93.299	0.057	0.041
PRc-37lg-25		0.021	0.011		0.040	0.059	72.437	20.823	93.395	0.081	0.040
PRc-37lg-27		0.020	0.016		0.039	0.045	70.907	20.388	91.426	0.065	0.039
PRc-37lg-28		0.035	0.009		0.041	0.051	71.816	20.653	92.609	0.085	0.041
PRc-37lg-29		0.131	0.009		0.044	0.050	71.918	20.771	92.931	0.181	0.044
PRc-37lg-30	0.010	0.150	0.031	0.040	0.043	0.043	70.199	20.345	90.860	0.194	0.084
PRc-73lg-1	0.010	0.014	0.016		0.064	0.043	72.196	20.764	93.107	0.057	0.064
PRc-73lg-2			0.014		0.064	0.048	72.206	20.763	93.115	0.048	0.064
PRc-73lg-3			0.014		0.064	0.043	71.897	20.670	92.704	0.043	0.064
PRc-73lg-4		0.015	0.009		0.067	0.046	72.208	20.759	93.110	0.060	0.067
PRc-73lg-5		0.185	0.007		0.065	0.047	72.174	20.895	93.374	0.232	0.065
PRc-73lg-6		0.014	0.010		0.067	0.048	72.104	20.729	92.977	0.062	0.067
PRc-73lg-7			0.014		0.066	0.045	72.185	20.754	93.082	0.045	0.066
PRc-73lg-8		0.013	0.011		0.064	0.042	72.135	20.738	93.011	0.056	0.064
PRc-73lg-9			0.013		0.064	0.045	72.167	20.744	93.046	0.045	0.064
PRc-73lg-10	0.009	0.058	0.014		0.065	0.046	72.023	20.753	92.969	0.103	0.065
PR-153c-lg-2			0.077		0.044	0.046	72.736	20.967	93.878	0.046	0.044
PR-153c-lg-3			0.013		0.044	0.042	72.711	20.877	93.686	0.042	0.044
PR-153c-lg-4			0.012		0.045	0.044	72.720	20.885	93.709	0.044	0.045
PR-153c-lg-5			0.029		0.044	0.047	72.711	20.902	93.737	0.047	0.044

PR-65c-lg-1	0.017	0.008			69.985	20.069	90.073	0.017	0.000	
PR-65c-lg-2	0.015	0.008	0.037	0.031	70.059	20.134	90.289	0.015	0.067	
PR-65c-lg-3	0.017	0.005		0.020	70.144	20.132	90.330	0.017	0.020	
PR-65c-lg-4	0.022	0.006		0.014	70.328	20.174	90.536	0.022	0.014	
PR-65c-lg-5	0.017	0.005			70.047	20.082	90.147	0.017	0.000	
PR-65c-lg-6	0.035	0.006			70.141	20.130	90.312	0.035	0.000	
PR-65c-lg-7	0.019	0.012			70.098	20.110	90.238	0.019	0.000	
PR-148a-dlg-1	0.032	0.026		0.033	0.008	69.910	20.103	90.113	0.040	0.033
PR-148a-dlg-2	0.023	0.010		0.031		70.206	20.156	90.425	0.023	0.031
PR-148a-dlg-3	0.025	0.032		0.033	0.009	70.163	20.173	90.431	0.034	0.033
PR-148a-dlg-4	0.024	0.008		0.032	0.012	70.354	20.200	90.625	0.036	0.032
PR-148a-dlg-5	0.034	0.028		0.033	0.011	69.985	20.123	90.205	0.045	0.033
PR-148a-dlg-6	0.030	0.067		0.031		69.589	20.053	89.773	0.030	0.031
PR-148a-dlg-7	0.017	0.010		0.033	0.012	70.267	20.168	90.497	0.028	0.033
PR-148a-dlg-8	0.022	0.031		0.028		68.353	19.664	88.129	0.037	0.028
PR-148a-dlg-9	0.029	0.030		0.035		70.179	20.177	90.449	0.029	0.035
PR-148a-dlg-10	0.041	0.064		0.031		69.668	20.082	89.890	0.041	0.031
PR-82Ad-dg-1	0.025	1.042		0.038	0.063	67.916	20.545	89.464	0.074	0.038
PR-82Ad-dg-2	0.015	0.859		0.039	0.066	68.247	20.404	89.435	0.066	0.039
PR-82Ad-dg-3	0.025	1.773		0.039	0.051	67.334	21.201	90.253	0.063	0.039
PR-82Ad-dg-4	0.023	1.165		0.036	0.061	67.641	20.613	89.383	0.076	0.036
PR-82Ad-dg-5		1.071		0.036	0.056	68.023	20.519	89.467	0.079	0.036
PR-82Ad-dg-6	0.011	0.886		0.038	0.054	67.875	20.305	88.960	0.067	0.038
PR-64Adc-dg-1		0.021		0.048	0.028	69.920	19.803	89.503	0.028	0.048

PR-64Adc-dg-2			0.015		0.051	0.031	69.905	19.802	89.498	0.031	0.051
PR-64Adc-dg-3			0.039		0.050	0.023	69.461	19.707	88.984	0.023	0.050
PR-64Adc-dg-4			0.061		0.050	0.026	69.215	19.802	89.020	0.026	0.050
PR-64Adc-dg-5			0.030		0.047	0.030	69.869	19.805	89.475	0.030	0.047
PR-64Adc-dg-6			0.025		0.050	0.030	70.281	19.945	90.053	0.030	0.050
PR-37dg-1			0.015	0.009	0.039	0.032	70.500	20.249	90.847	0.032	0.047
PR-37dg-2			0.011		0.042	0.030	69.776	20.045	89.922	0.030	0.042
PR-37dg-3	0.029	0.021		0.024	0.043	0.049	70.311	20.247	90.731	0.078	0.066
PR-37dg-4	0.066	0.011			0.039	0.022	70.178	20.201	90.517	0.088	0.039
PR-37dg-5	0.041	0.069	0.020	0.011	0.042	0.020	69.715	20.126	90.066	0.109	0.053
PR-37dg-6		0.021	0.031	0.014	0.044	0.046	69.132	19.905	89.198	0.067	0.058
PR-37dg-7	0.017	0.084	0.010		0.039	0.019	69.171	19.940	89.281	0.103	0.039
PR-37dg-8			0.023	0.013	0.039	0.035	69.176	19.881	89.167	0.035	0.052
PR-37dg-9		0.026	0.025		0.041	0.009	69.667	20.035	89.805	0.035	0.041
PR-37dg-10		0.022			0.037	0.018	69.697	20.013	89.785	0.040	0.037
PR-37dg-11		0.017	0.007		0.042	0.051	72.063	20.707	92.892	0.068	0.042
PR-37dg-12		0.026	0.012		0.041	0.025	70.339	20.220	90.670	0.051	0.041
PR-37dg-13		0.024	0.012		0.041	0.055	69.418	19.984	89.591	0.129	0.041
PR-37dg-14		0.047	0.016		0.039	0.044	69.063	19.882	89.095	0.091	0.039
PR-37dg-15		0.012	0.016		0.040	0.057	69.399	19.950	89.475	0.070	0.040
PR-37dg-16		0.033	0.016		0.042	0.091	69.304	19.959	89.460	0.124	0.042
PR-37dg-17		0.219	0.021	0.012	0.040	0.038	69.561	20.195	90.104	0.268	0.053
PR-37dg-18		0.034	0.022		0.043	0.021	71.175	20.480	91.786	0.055	0.043
PR-37dg-20		0.131	0.017	0.014	0.042	0.009	69.563	20.096	89.868	0.141	0.055

PR-37dg-21		0.044	0.015		0.041	0.048	69.461	19.995	89.610	0.092	0.041
PR-37dg-22	0.028	0.043	0.078		0.038	0.041	68.702	19.900	88.935	0.189	0.038
PR-37dg-23		0.022	0.010		0.038	0.013	70.162	20.155	90.403	0.035	0.038
PR-37dg-24		0.022	0.019		0.040	0.018	69.629	20.017	89.749	0.040	0.040
PR-37dg-25		0.015	0.017		0.037	0.046	69.530	19.987	89.635	0.061	0.037
PR-37dg-26		0.019	0.021		0.041	0.031	69.462	19.969	89.540	0.049	0.041
PR-37dg-27		0.036	0.021		0.037	0.026	69.595	20.025	89.745	0.062	0.037
PR-37dg-28		0.020	0.009		0.039	0.025	70.830	20.347	91.270	0.045	0.039
PR-37dg-29		0.014	0.021	0.016	0.038	0.017	69.304	19.929	89.343	0.031	0.054
PR-37dg-30		0.350	0.015		0.039	0.037	69.087	20.157	89.700	0.386	0.039
PRb-37dg-1	0.018	0.271	0.036		0.035	0.051	69.501	20.235	90.144	0.322	0.035
PRb-37dg-2		0.024	0.017		0.040	0.016	69.867	20.086	90.056	0.040	0.040
PRb-37dg-3	0.029	0.053	0.040		0.041	0.032	70.084	20.219	90.496	0.085	0.041
PRb-37dg-4		0.037	0.008		0.040	0.043	70.110	20.157	90.389	0.080	0.040
PRb-37dg-5		0.155	0.010		0.043		70.255	20.298	90.766	0.155	0.043
PRb-37dg-6		0.025	0.011		0.039	0.039	69.900	20.092	90.105	0.064	0.039
PRb-37dg-7		0.201	0.011		0.039		69.781	20.207	90.248	0.201	0.039
PRb-37dg-8		0.042	0.008		0.042	0.024	70.570	20.292	90.980	0.066	0.042
PRb-37dg-9	0.017	0.091	0.054	0.020	0.041		69.885	20.210	90.326	0.091	0.062
PRb-37dg-10		0.024	0.017		0.041	0.023	70.818	20.358	91.284	0.047	0.041
PRc-73dg-1		0.050	0.009		0.070		69.802	20.089	90.023	0.050	0.070
PRc-73dg-2		0.041			0.062		69.901	20.087	90.084	0.041	0.062
PRc-73dg-3		0.032	0.006		0.075	0.011	69.638	20.025	89.786	0.043	0.075
PRc-73dg-4	0.008	0.034	0.011		0.058		69.295	19.929	89.336	0.034	0.058

PRc-73dg-5		0.037	0.012		0.064	69.603	20.024	89.752	0.037	0.064
PRc-73dg-6		0.035	0.016		0.072	69.788	20.083	90.001	0.035	0.072
PRc-73dg-7		0.032	0.008		0.064	69.661	20.027	89.793	0.032	0.064
PRc-73dg-8		0.075	0.008		0.081	69.464	20.017	89.647	0.075	0.081
PRc-73dg-9		0.333	0.007		0.062	70.055	20.410	90.882	0.333	0.062
PRc-73dg-10		0.046	0.011		0.067	69.540	20.023	89.725	0.074	0.067
PR-153c-1		0.027	0.009		0.045	70.338	20.198	90.609	0.027	0.045
PR-153c-2		0.022	0.008		0.045	70.188	20.147	90.397	0.022	0.045
PR-153c-3		0.064	0.008		0.062	0.011	70.390	20.256	90.781	0.074
PR-153c-4		0.042	0.019		0.067	0.026	70.524	20.298	90.970	0.068
PR-153c-5		0.016	0.009		0.044		70.583	20.262	90.911	0.016
PR-153c-6		0.507	0.013		0.043	0.043	71.771	21.062	93.446	0.550
PR-77Aa-1	0.038	0.117	0.039		0.041	0.036	71.670	20.756	92.744	0.193
PR-77Aa-2		0.031	0.016		0.046	0.036	71.882	20.674	92.689	0.067
PR-77Aa-3			0.009		0.052	0.038	71.917	20.653	92.674	0.038
PR-77Aa-4	0.021		0.033		0.041	0.033	70.522	20.238	90.791	0.033
PR-77Aa-5		0.028			0.052	0.043	72.279	20.643	92.907	0.071
PR-144ax-06		0.049	0.014		0.034		70.266	20.206	90.567	0.049
PR-144ax-08			0.012		0.045	0.031	72.282	20.760	93.136	0.031
PR-144ax-09		0.033	0.014	0.072	0.066		69.741	20.102	90.020	0.033
PR-144ax-010		0.023	0.012		0.032		69.933	20.079	90.068	0.023
PR-144ax-012 line		0.023	0.009		0.045		70.056	20.122	90.249	0.023
PR-144ax-012 line		0.026	0.013	0.010	0.041		69.845	20.071	90.000	0.026
PR-144ax-012 line		0.017	0.014		0.040		69.879	20.071	90.022	0.017

PR-144ax-012 line		0.092	0.026	0.009	0.080	69.192	19.980	89.383	0.092	0.089	
PR-144ax-012 line	0.053	0.018	0.060		0.046	69.676	20.106	89.964	0.018	0.046	
PR-144ax-012 line		0.028	0.006		0.047	70.026	20.115	90.219	0.028	0.047	
PR-144ax-012 line		0.081	0.014	0.027	0.054	68.675	19.810	88.670	0.081	0.081	
PR-144ax-012 line		0.085	0.005		0.081	69.655	20.073	89.892	0.085	0.081	
PR-144ax-012 line		0.025	0.011	0.014	0.033	69.831	20.059	89.963	0.025	0.046	
PR-144ax-012 line		0.088	0.009		0.083	69.449	20.026	89.655	0.088	0.083	
PR-144bx-02	0.011	0.028	0.013	0.011	0.045	69.991	20.125	90.218	0.028	0.056	
PR-144bx-03		0.049	0.006	0.017	0.107	69.787	20.105	90.072	0.049	0.124	
PR-144bx-04		0.020	0.008	0.014	0.015	69.986	20.089	90.123	0.020	0.028	
PR-144bx-05		0.040	0.010		0.023	69.509	19.975	89.560	0.040	0.023	
PR-144bx-06		0.058	0.010	0.018	0.088	69.717	20.087	89.975	0.058	0.107	
PR-144by-010					0.014	70.279	20.151	90.451	0.000	0.014	
PR-144by-012 line		0.051	0.019	0.021	0.096	69.572	20.064	89.832	0.051	0.117	
PR-144by-012 line		0.027	0.010	0.044	0.077	69.671	20.060	89.886	0.027	0.121	
PR-144by-012 line		0.024	0.019		0.053	70.525	20.279	90.906	0.024	0.053	
PR-144by-012 line		0.023	0.011	0.012	0.045	69.592	20.000	89.681	0.023	0.057	
PR-144by-012 line		0.044	0.020		0.049	69.543	20.016	89.681	0.044	0.049	
PR-144by-012 line		0.089	0.012	0.012	0.046	69.652	20.078	89.889	0.089	0.058	
PR-144by-012 line		0.025	0.010	0.059	0.058	69.759	20.083	89.988	0.025	0.117	
PR-144by-012 line			0.007		0.014	69.720	19.999	89.747	0.000	0.014	
PR-144by-012 line		0.040	0.007	0.058	0.104	69.445	20.028	89.686	0.040	0.162	
PR-144cx-01			0.015		0.039	0.012	72.132	20.709	92.913	0.012	0.039
PR-144cx-02		0.047	0.008		0.028	69.808	20.061	89.946	0.047	0.028	

PR-144cx-03		0.015	0.010		0.041		72.391	20.784	93.244	0.015	0.041
PR-144cx-04		0.040	0.009	0.012	0.057		69.772	20.068	89.956	0.040	0.069
PR-144cx-05		0.082	0.013	0.011	0.063		69.864	20.135	90.160	0.082	0.074
PR-144cy-06		0.039	0.011		0.016		69.878	20.074	90.013	0.039	0.016
PR-144cy-012 line		0.030	0.011	0.017	0.050		69.947	20.115	90.171	0.030	0.067
PR-144cy-012 line		0.051	0.008	0.082	0.059		69.854	20.144	90.188	0.051	0.140
PR-144cy-012 line		0.049	0.010		0.041		69.542	19.998	89.640	0.049	0.041
PR-144cy-012 line		0.020	0.006	0.063	0.050		69.497	19.995	89.618	0.020	0.113
PR-144cy-012 line	0.209	0.135	0.177	0.015	0.045		69.265	20.337	90.189	0.135	0.060
PR-144cy-012 line		0.020	0.010	0.011	0.052		69.715	20.033	89.839	0.020	0.062
PR-144cy-012 line		0.018	0.013	0.051	0.035		69.787	20.068	89.959	0.018	0.087
PR-144cz-13			0.012		0.041		72.344	20.772	93.187	0.000	0.041
PR-144cz-14			0.008		0.045		72.259	20.754	93.106	0.020	0.045
PR-144cz-15			0.009		0.042	0.038	72.350	20.779	93.232	0.038	0.042
PR-144cz-16			0.023		0.038	0.045	72.248	20.769	93.137	0.045	0.038
PR-144cz-17	0.022	0.010			0.044		72.586	20.851	93.519	0.022	0.044
PR-144cz-18			0.007		0.043		72.592	20.842	93.509	0.001	0.043
PR-144cz-19			0.011		0.045	0.033	72.678	20.868	93.636	0.033	0.045
PR-144cz-20	0.016	0.010			0.044	0.024	72.437	20.816	93.360	0.041	0.044
PR-144cz-23			0.013		0.041	0.012	72.407	20.794	93.283	0.012	0.041
PR-144cz-24			0.011		0.041		72.512	20.820	93.404	0.000	0.041
PR-144cz-25	0.020	0.009		0.056	0.046	0.014	72.542	20.872	93.555	0.034	0.102
PR-144cz-28			0.013	0.085	0.033	0.010	72.612	20.903	93.667	0.010	0.119
PR-144cz-29			0.010	0.039	0.044	0.017	72.640	20.882	93.639	0.017	0.082

PR-144cz-32			0.011		0.092	0.041		72.338	20.833	93.338	0.000	0.132
PR-144cz-33			0.010			0.041		72.417	20.791	93.277	0.000	0.041
PR-144cz-34			0.010			0.041	0.015	72.585	20.832	93.484	0.015	0.041
PR-144cz-35			0.009			0.043	0.018	72.261	20.744	93.082	0.018	0.043
PR-144cx-36	0.032		0.009		0.010	0.029		70.160	20.155	90.389	0.032	0.039
PR-144cx-37	0.026		0.010		0.009	0.046		69.842	20.064	89.983	0.026	0.055
PR-144cx-38	0.046		0.010		0.031	0.067		69.807	20.100	90.055	0.046	0.098
PR-144cx-39	0.031		0.006		0.054	0.048		69.917	20.133	90.206	0.031	0.103
PR-144cx-41	0.030		0.009		0.077	0.034		70.211	20.216	90.570	0.030	0.112
PR-144cx-42	0.030		0.012		0.013	0.054		70.140	20.165	90.406	0.030	0.068
PR-144cx-44	0.032		0.008		0.076	0.049		69.926	20.142	90.230	0.032	0.125
PR-144cx-45	0.016		0.010		0.003	0.049		69.889	20.073	90.043	0.016	0.052
PR-144cx-46	0.035		0.009			0.069		70.363	20.235	90.712	0.035	0.069
PR-144cx-47	0.061		0.007			0.036		70.355	20.232	90.682	0.061	0.036
PR-144cx-48	0.021		0.007		0.009	0.046		69.807	20.053	89.941	0.021	0.055
PR-82ax-01						0.046	0.048	72.225	20.750	93.104	0.070	0.046
PR-82ax-04	0.020	0.089	0.221			0.049	0.048	71.572	20.890	92.892	0.137	0.049
PR-82ax-05		0.016	0.007			0.046	0.047	72.031	20.695	92.842	0.063	0.046
PR-82ax-06			0.011			0.047	0.049	72.126	20.721	92.961	0.049	0.047
PR-82ax-07		0.014	0.007			0.047	0.052	72.261	20.762	93.145	0.066	0.047
PR-82ax-08		0.014	0.006			0.046	0.051	72.239	20.754	93.112	0.065	0.046
PR-82ax-09		0.018	0.005			0.046	0.053	72.206	20.744	93.068	0.070	0.046
PR-82ax-010		0.025	0.020			0.051	0.053	72.165	20.756	93.062	0.078	0.051
PR-82ax-011		0.018	0.008			0.043	0.050	71.982	20.682	92.782	0.068	0.043

PR-82ax-012	0.022	0.008	0.006	0.044	0.050	72.061	20.706	92.886	0.072	0.050
PR-82ax-013		0.006		0.048	0.045	72.265	20.756	93.133	0.045	0.048
PR-82ax-014	0.017	0.007		0.046	0.048	71.986	20.682	92.785	0.065	0.046
PR-82ax-015	0.014			0.049	0.048	71.971	20.667	92.741	0.062	0.049
PR-82ax-018		0.007		0.048	0.047	72.153	20.732	93.011	0.047	0.048
PR-82ax-019	0.019	0.011		0.044	0.050	71.713	20.614	92.457	0.068	0.044
PR-82ax-020	0.021	0.008		0.051	0.044	72.132	20.726	92.977	0.065	0.051
PR-82ax-021		0.006		0.051	0.046	72.422	20.804	93.344	0.046	0.051
PR-82ax-022	0.013	0.016		0.046	0.049	71.815	20.639	92.575	0.062	0.046
PR-82ay-024	0.018	0.012	0.009	0.045	0.036	69.795	20.067	89.990	0.053	0.055
PR-82ay-025	0.014	0.015		0.046	0.037	69.914	20.093	90.119	0.050	0.046
PR-82ay-029	0.038	0.072		0.047	0.031	69.272	20.000	89.474	0.083	0.047
PR-82ay-032	0.022	0.035		0.048	0.023	69.558	20.021	89.716	0.045	0.048
PR-82ay-033	0.095	0.060	0.026	0.039	0.020	69.330	20.057	89.626	0.116	0.065
PR-82ay-034	0.024	0.033	0.006	0.049	0.033	69.349	19.967	89.471	0.070	0.055
PR-82ay-035	0.020	0.030		0.047	0.038	69.637	20.039	89.818	0.057	0.047
PR-82ay-036	0.024	0.036		0.049	0.026	69.578	20.024	89.733	0.050	0.049
PR-82ex-039		0.008		0.047	0.047	72.026	20.686	92.821	0.047	0.047
PR-82ex-040		0.010		0.044	0.043	72.229	20.744	93.075	0.043	0.044
PR-82ex-041		0.007	0.061	0.043	0.044	72.072	20.737	92.969	0.044	0.103
PR-82ex-042		0.007		0.047	0.051	72.434	20.806	93.355	0.051	0.047
PR-82ex-043	0.009	0.062	0.737	0.049	0.062	70.941	21.275	93.152	0.137	0.049
PR-82ex-044	0.008	0.034	0.363	0.047	0.042	71.905	21.086	93.486	0.076	0.047
PR-82ex-045		0.010		0.049	0.049	72.214	20.748	93.081	0.049	0.049

PR-82ey-046	0.051	0.079	0.022	0.046	0.028	69.437	20.077	89.753	0.101	0.067
PR-82ey-047		0.016	0.049	0.049	0.050	69.740	20.079	89.994	0.050	0.097
PR-82ey-048		0.008	0.009	0.046	0.038	69.907	20.083	90.099	0.038	0.055
PR-82ey-049		0.008		0.045	0.043	70.100	20.138	90.346	0.043	0.045
PR-82ey-050		0.011		0.046	0.043	69.565	19.987	89.662	0.043	0.046
PR-82ey-051		0.015		0.048	0.046	70.033	20.127	90.278	0.046	0.048
PR-82ey-052	0.016	0.009		0.045	0.039	69.988	20.108	90.202	0.055	0.045
PR-73ax-01		0.007		0.062	0.041	72.307	20.770	93.194	0.041	0.062
PR-73ax-02	0.070	0.104		0.062	0.037	71.766	20.784	92.826	0.106	0.062
PR-73ax-03		0.013		0.062	0.040	72.391	20.802	93.316	0.040	0.062
PR-73ax-04	0.014	0.007		0.065	0.040	72.164	20.737	93.026	0.054	0.065
PR-73ax-05		0.006		0.061	0.041	72.230	20.748	93.094	0.041	0.061
PR-73ax-06	0.014	0.007		0.061	0.036	72.399	20.797	93.305	0.050	0.061
PR-73ay-07	0.026	0.033	0.016		0.062	69.877	20.121	90.153	0.044	0.062
PR-73ay-08		0.023	0.010	0.017	0.029	70.096	20.137	90.311	0.023	0.047
PR-73ay-09		0.020	0.019		0.038	69.846	20.070	89.998	0.020	0.038
PR-73ay-010		0.067	0.013	0.011	0.069	70.031	20.174	90.361	0.067	0.080
PR-73bx-01		0.011		0.061	0.038	72.067	20.708	92.895	0.038	0.061
PR-73bx-02		0.009		0.061	0.038	72.347	20.787	93.255	0.038	0.061
PR-73bx-03	0.017	0.009		0.062	0.040	72.219	20.759	93.109	0.057	0.062
PR-73bx-04	0.024	0.018		0.062	0.045	72.196	20.772	93.125	0.069	0.062
PR-73bx-05		0.010		0.061	0.041	72.296	20.766	93.175	0.041	0.061
PR-73bx-06		0.013		0.062	0.039	72.181	20.744	93.051	0.039	0.062
PR-73bx-07		0.007		0.060		69.850	20.073	90.026	0.000	0.060

PR-73bx-08		0.043	0.013		0.060	0.041	71.894	20.693	92.749	0.084	0.060
PR-73bx-011		0.030	0.015		0.065		69.745	20.113	90.109	0.164	0.065
PR-73bx-012	0.009	0.158	0.018		0.059	0.039	71.155	20.594	92.037	0.199	0.059
PR-73dx-01			0.005		0.061	0.040	72.017	20.687	92.817	0.040	0.061
PR-73dx-02			0.010		0.055	0.039	71.968	20.676	92.757	0.039	0.055
PR-73dx-03			0.006		0.062	0.041	72.085	20.708	92.913	0.041	0.062
PR-73dx-04			0.007	0.009	0.061	0.039	72.308	20.776	93.205	0.039	0.070
PR-73dx-05			0.009		0.061	0.043	72.118	20.717	92.950	0.043	0.061
PR-73dx-06			0.007		0.063	0.038	72.108	20.712	92.933	0.038	0.063
PR-73dx-07			0.007		0.062	0.038	71.987	20.686	92.797	0.038	0.062
PR-73dy-08		0.059	0.009		0.062	0.038	72.341	20.839	93.365	0.097	0.062
PR-73dy-09			0.006	0.060	0.061	0.038	72.610	20.894	93.672	0.038	0.121
PR-73dy-010			0.009	0.010	0.061	0.037	72.342	20.783	93.238	0.037	0.071
PR-73dy-011		0.013	0.010		0.062	0.038	72.239	20.760	93.122	0.052	0.062
PR-73dy-012			0.006		0.063	0.041	72.611	20.860	93.591	0.041	0.063
PR-73dy-013			0.007		0.065	0.043	72.259	20.771	93.170	0.043	0.065
PR-73dy-014		0.014	0.010		0.063	0.038	72.321	20.787	93.238	0.052	0.063
PR-73dy-015			0.009		0.060	0.041	72.749	20.910	93.791	0.041	0.060
PR-73dy-016			0.006		0.060	0.038	72.455	20.806	93.366	0.038	0.060
PR-73dz-022		0.016		0.071	0.070		69.961	20.144	90.271	0.016	0.141
PR-65ax-01			0.007		0.036		69.977	20.077	90.100	0.000	0.036
PR-65ax-02			0.005		0.022		69.970	20.078	90.097	0.000	0.022
PR-65ax-07		0.025	0.006	0.027	0.062		70.238	20.188	90.526	0.025	0.090
PR-65ax-08			0.005	0.022	0.053		69.893	20.074	90.048	0.000	0.075

PR-65ax-011		0.006		0.072		69.672	20.008	89.766	0.000	0.072
PR-65ax-012	0.031	0.007	0.092	0.075		69.559	20.059	89.816	0.031	0.167
PR-65ax-015				0.042		70.049	20.093	90.186	0.000	0.042
PR-65ax-016		0.007		0.037		69.998	20.085	90.132	0.000	0.037
PR-65ax-017		0.010	0.018	0.034		69.494	19.953	89.511	0.000	0.052
PR-65ax-018		0.011				70.060	20.092	90.171	0.000	0.000
PR-65ax-021		0.011	0.019	0.054		69.667	20.015	89.769	0.000	0.073
PR-65ax-022	0.013	0.007	0.087	0.086		70.003	20.169	90.355	0.013	0.173
PR-65ay-024		0.021		0.052	0.046	72.120	20.729	92.969	0.046	0.052
PR-65ay-025		0.023		0.047	0.054	71.967	20.694	92.798	0.054	0.047
PR-65ay-027		0.010		0.043	0.049	72.265	20.745	93.101	0.049	0.043
PR-65ay-028		0.008		0.050	0.048	71.808	20.714	92.855	0.262	0.050
PR-65ay-029	0.014	0.020		0.050	0.048	72.073	20.724	92.932	0.062	0.050
PR-65ay-030		0.013		0.049	0.050	72.217	20.744	93.073	0.050	0.049
PR-65ay-031	0.009	0.035	0.070	0.047	0.052	72.065	20.804	93.088	0.087	0.047
PR-65ay-032		0.014	0.034	0.055	0.049	71.711	20.630	92.481	0.063	0.055
PR-65ay-033		0.010	0.056	0.053	0.056	71.955	20.706	92.835	0.056	0.108
PR-65ay-034		0.010		0.050	0.060	72.353	20.792	93.279	0.060	0.050
PR-65ay-035		0.006		0.049	0.053	72.173	20.728	93.014	0.053	0.049
PR-65ay-036		0.007		0.049	0.048	72.069	20.698	92.877	0.048	0.049
PR-65ay-037		0.012		0.045	0.052	72.181	20.734	93.028	0.052	0.045
PR-65ay-038		0.008		0.048	0.055	72.495	20.816	93.417	0.055	0.048
PR-65ay-039	0.058	0.009		0.050	0.051	72.504	20.866	93.524	0.110	0.050
PR-65ay-040		0.009		0.050	0.044	72.548	20.835	93.490	0.044	0.050

